Alexandra Herg, BSc

Petrologische Untersuchung der Eoalpinen Metamorphose südlich der Koralpe

MASTERARBEIT

Zur Erlangung des akademischen Grades

Master of Sciences

Masterstudium Erdwissenschaften

eingereicht an der

Technischen Universität Graz

Betreuer

Ao.Univ.-Prof. Mag.rer.nat. Dr. Kurt Stüwe

Institut für Erdwissenschaften

Universitätsplatz 2, A-8010 Graz

Graz, Oktober 2017

EIDESSTATTLICHE ERKLÄRUNG

Ich erkläre an Eides statt, dass ich die vorliegende Arbeit selbstständig verfasst, andere als die angegebenen Quellen/Hilfsmittel nicht benutzt, und die den benutzten Quellen wörtlich und inhaltlich entnommenen Stellen als solche kenntlich gemacht habe. Das in TUGRAZonline hochgeladene Textdokument ist mit der vorliegenden Masterarbeit identisch.

28.10.2017

Alexandra Herg

Datum

Unterschrift

ACKNOWLEDGEMENTS

First and foremost I want to thank my supervisor Kurt Stüwe for his great assistance and countless hints in the right direction. Thank you for giving me many new ideas and introducing me to scientific working. I would also like to thank Karl Ettinger and Jürgen Neubauer who assisted me during the many days of work at the electron microscope. Anton Pock is thanked for his help during laboratory work and Georg Stegmüller is thanked for solving technical problems. Roger Powell, Ralf Schuster, Veronika Tenczer and Richard White are thanked for advice and help on specific questions regarding details of the geothermobarometric calculations and the interpretation of results. Simon Schorn deserves great credit for always replying to my questions and especially for the assistance with creating pseudosections. Special thanks also go to all my friends and colleagues for discussions, moral support and understanding during busy times. Anna, Elli, Maresi, Flo as well as Theres, Steffi, Carola and Gregor are thanked for all those great and exciting years spent together at university as well as for our joint activities and travels. Last but not least I want to thank my family for their moral and financial assistance as well as countless travels over the years. Thank you for your support.

ABSTRACT

The southern Pohorje Mountains of Slovenia preserve the highest recorded pressures of the Cretaceous metamorphic event in the Alps (up to 40 kbar at 900 °C). The Plankogel Unit to the North exhibits significantly lower grade metamorphic conditions (7.1 ± 1.95 – 11.5 ± 3.42 kbar at 650 °C), but eclogite facies rocks reappear north of the Plankogel Unit in the Koralpe Complex (around 20 kbar at 700 °C). In view of the fact that both the Koralpe and the Pohorje Complex have been interpreted as evidence for crustal scale slab extraction processes the position of the Plankogel Unit remains enigmatic. In order to contribute to this debate I present a metamorphic field gradient from the Koralpe to the Pohorje Mountains across the Plankogel Unit. The data affirm that the pressures gradually increase from the Koralpe to the Pohorje Mountains, with an interruption caused by the Plankogel Unit. Moreover, in the Pohorje Mountains, peak metamorphic conditions (explored with the garnet-muscovite-kyanite-quartz assemblage) exhibit pressures from 16.2 ± 3.45 kbar to 23.9 ± 2.49 kbar at 700 °C, but decompression and cooling conditions for metapelites calculated with the total assemblage yield 9.7 ± 2.54 kbar to 12.9 ± 1.83 kbar at 650 °C suggesting a hiatus in the exhumation history. I interpret the data to reflect rapid exhumation of the high- to ultrahigh pressure rocks located in the footwall of the subducting slab in both the Koralpe and the Pohorje Mountains caused by slab extraction. At mid-crustal level the rocks partly re-equilibrated before they experienced a second exhumation. During the final exhumation Koralpe and Pohorje are suggested to have been separated by an east-west trending fault system with the Plankogel Unit remaining in the hanging wall of the Pohorje Mountains.

ZUSAMMENFASSUNG

Das südliche Pohorje Gebirge weist die höchsten nachgewiesenen Drucke des kretazischen metamorphen Ereignisses in den Alpen auf (bis zu 40 kbar bei 900 °C). Die Plankogel Einheit im Norden hingegen zeigt wesentlich niedrigere metamorphe Bedingungen (7.1 ± 1.95 – 11.5 ± 3.42 kbar bei 650 °C). Nördlich davon tauchen jedoch im Koralpe Komplex abermals Eklogit-fazielle Gesteine mit Drucken von ungefähr 20 kbar bei 700 °C auf. Angesichts der Tatsache, dass sowohl Koralpe als auch Pohorje Komplex als Beweis für einen *slab extraction* Prozess angesehen werden, bleibt die Rolle der Plankogel Einheit ungeklärt. Um der Aufklärung dieser Diskussion beizutragen, wird in dieser Arbeit ein metamorpher Feldgradient von der Koralpe über die Plankogel Einheit bis zum Pohorje Gebirge ermittelt. Die Daten bestätigen einen graduellen Anstieg der Drucke von der Koralpe bis ins Pohorje Gebirge, mit einer von der Plankogel Einheit bedingten Unterbrechung. Darüber hinaus zeigen Berechnungen für die maximalen Metamorphosebedingungen mit der Mineralparagenese Granat-Muskovit-Kyanit-Quarz Drucke von 16.2 ± 3.45 kbar bis 23.9 ± 2.49 kbar bei 700 °C und Berechnungen mit der Gesamtparagenese Drucke von 9.7 ± 2.54 kbar bis 12.9 ± 1.83 kbar bei 650 °C für die Dekompressions- und Abkühlungsbedingungen. Diese Daten deuten auf eine Lücke in der Exhumierungsgeschichte dieser Region hin. Die Daten werden dahingehend interpretiert, dass die Exhumierung der sich im Liegenden der abtauchenden Platte befindlichen Hoch- und Ultrahochdruckgesteine der Koralpe und des Pohorje Gebirges von einer *slab extraction* bedingt wurde. In der mittleren Kruste konnten die Gesteine teilweise reäquilibrieren, bevor sie eine weitere Exhumierung erfuhren. Es wird vorgeschlagen, dass Koralpe und Pohorje während dieser letzten Phase der Exhumierung durch ein Ost-West verlaufendes Störungssystem getrennt wurden, wobei sich die Plankogel Einheit im Hangenden des Pohorje Gebirges befindet.

CONTENT

1 INTRODUCTION

Slab extraction on an orogenic scale describes the downward removal of a large body of rocks within a subduction zone (Froitzheim et al., 2003, 2006). This concept has been proposed for the Saualpe-Koralpe-Pohorje complexes as an explanation for the exhumation of deeply subducted rocks (e.g. Janák et al., 2004, 2006, 2009, 2015; De Hoog et al., 2009). The east-west-striking and southward dipping Plattengneis-Plankogel shear zone was recently suggested to be the trace of the slab extracted in the context of Eoalpine subduction (Schorn & Stüwe, 2016). Pressures decrease across this detachment from 23 – 24 kbar (determined for the eclogite facies unit in the north lying footwall of the shear zone) to 12 – 14 kbar (measured for the south-lying amphibolite facies metapelites in the hanging wall; Schorn & Stüwe, 2016). Interestingly, pressures appear to be increasing again further south in the Pohorje Mountains. The southeasternmost part of this area is occupied by the Slovenska Bistrica ultramafic complex which yields pressures of up to 40 kbar for garnet peridotites (Janák et al., 2006; De Hoog et al., 2009).

The reappearance of high-pressure rocks southwards of the hanging wall of the inferred extraction fault raises the questions of what role the slab extraction played in regard to the exhumation of high- and ultrahigh-pressure rocks in the Pohorje area and to what extent the Saualpe, Koralpe and Pohorje share a common tectonic history. Answers to this puzzle can be supported by a careful documentation of the metamorphic field gradient from the southern Koralpe area to the Pohorje Mountains.

The transect between high-grade metapelites of the Koralpe and Pohorje Mountains is interrupted by several different units which complicates the task. To the West the Pohorje is overlain by units of low-grade metasediments and sediments. The central part of the mountains is occupied by a Miocene intrusion (Fodor et al., 2008; Trajanova et al., 2008). To the North of the intrusion, the Ribnica Trough superimposes the metapelites and to the South and East the whole complex dips below the sediments of the Pannonian Basin.

Nevertheless, a number of samples were taken from the metapelites throughout the investigated area. Petrographic analyses and mineral chemical analyses were performed on selected samples. Formation pressure conditions were calculated at defined temperatures with the program THERMOCALC. The results were projected along a transect from Northwest to Southeast through the Pohorje Mountains.

The determined metamorphic field gradient for the metapelites in the Plankogel Unit and the Pohorje Mountains suggests a new interpretation for the tectonic history and exhumation of the Saualpe-Koralpe-Pohorje area. In particular, two different models are compared and discussed.

2 GEOLOGICAL SETTING

2.1 Geography and Lithologies

The southeasternmost exposure of the Eastern Alps is represented by the Pohorje (Bachern) Mountains. They are interpreted to be the most deeply subducted part of the Alps during the Cretaceous orogeny (Janák et al., 2004, 2005, 2006, 2009, 2015; Thöni, 2006; Miller et al., 2007; Kirst et al., 2010). The research area comprises these mountains as well as parts of the Kozjak (Possruck) Mountains and the southernmost area of the Koralpe (Figs. 1 & 2). In the Southwest of the research area, the Periadriatic Lineament is offset by the Labot (Lavanttal) Fault. The Labot Fault separates the Pohorje Mountains from the Karavanke Mountains in the West. To the East and South, the metamorphic Pohorje Complex gently dips below the Neogene sediments of the Pannonian Basin (Fodor et al., 2003). Toward the North, the Drava river channel separates the Pohorje from the Kozjak Mountains as well as the Koralpe region.

Several studies used conventional geothermobarometry alongside other methods to describe the pressure conditions of the research area. Overall the field gradient is characterized by increasing metamorphic grade from the Koralpe Complex to the South of the Pohorje Mountains. There are, however, unclear pressure conditions throughout the metapelites of the Pohorje Mountains, as well as an interruption of high-grade conditions caused by the Plankogel Unit, which remain the subject of this study.

The most deeply subducted part lies in the very South of the research area and is represented by the Slovenska Bistrica ultramafic complex ("Slovenska Bistrica ultramafic complex – SBUC" after Janák et al., 2006). The eclogites in this part of the Pohorje Mountains yielded peak metamorphic conditions at 30 – 31 kbar and 760 – 825 °C (Janák et al., 2004) and 30 – 37 kbar and 710 – 940 °C (Vrabec et al., 2012), whereas the garnet peridotites were metamorphosed at 40 kbar and around 900 °C (Janák et al., 2006; De Hoog et al., 2009). Earlier studies, on the other hand, had determined lower conditions at 18 – 25 kbar and 630 – 700 °C (Sassi et al., 2004) and >21 kbar and <750 °C (Miller et al., 2005) for eclogites. Since then, Janák et al. (2015) could verify UHP conditions by investigating diamonds in both, eclogites and gneisses, of the SBUC area.

The metapelites in close vicinity of the SBUC have also been a subject matter of geothermobarometric calculations in several studies. For the peak metamorphic assemblage of metapelites, values of 27.5 kbar at 780 °C (Hurai et al., 2010) and 21 – 27 kbar at

700 – 800 °C (Janák et al., 2009) were calculated. The decompression conditions were determined at about 9 kbar at 720 °C (Hurai et al., 2010) and 5 kbar at 550 °C (Janák et al., 2009). In comparison to these values, eclogites in the Koralpe region have yielded pressures of around 20 kbar at 700 °C (Hoinkes et al., 1999), which indicates a rise in pressures from the Koralpe to the SBUC region.

However, the Plankogel detachment represents an interruption of this increase in metamorphic conditions. Pressures determined for the Cretaceous event in this unit are generally between 7 – 10 kbar with temperatures of 550 – 600 °C and around 5 kbar and 540 °C for the Permian event (Gregurek et al., 1997; Thöni & Miller, 2009).

The Plankogel detachment is an east-west striking and southward dipping detachment juxtaposing the eclogite facies rocks of the Koralpe towards the amphibolite facies rocks further south (Gregurek et al., 1997; Tenczer & Stüwe et al., 2003; Eberlei et al., 2014). The Plankogel Unit consists of an approximately 400 m thick sequence of mainly garnet-micaschists (Gregurek et al., 1997). Since it had been less intensely metamorphosed during the Eoalpine event, some garnet cores still preserve relics of the Permian metamorphic event (Thöni & Miller, 2009). In contrast to the Plankogel Unit, the Koralpe exhibits a 1 km thick sequence of quartzo-feldspatic lithologies including the Plattengneis zone and several lenses of eclogites and metagabbros.

The Pohorje Mountains consist of a nappe stack containing three units. The basal nappe is referred to as the Pohorje Nappe ("Pohorje Nappe" after Janák et al., 2006) and is built up by medium- to high-grade metamorphic rocks. It belongs to the Lower Central Austroalpine (Janák et al., 2004) or the Koralpe-Wölz nappe system (Schmid et al., 2004) and is dominated by micaschists and gneisses including common and widely distributed lenses and bodies of eclogites, amphibolites, marbles, and metaquartzites (Hinterlechner-Ravnik, 1977; Jarc & Zupancic, 2009). The Pohorje Nappe also includes the metaultrabasic rocks of the SBUC. The middle and uppermost nappes are Upper Central Austroalpine units (Drauzug – Gurktal nappe system) and are confined to the northwestern part of the Pohorje Mountains. The middle unit superimposes the Pohorje Nappe and consists of low-grade Paleozoic metasediments and relics of a Permo-Mesozoic cover (Hinterlechner-Ravnik, 1977; Hurai et al., 2010). The slates and phyllites of this nappe are overlain by the uppermost unit containing unmetamorphosed Permo-Triassic and Senonian sediments (Hinterlechner-Ravnik, 1977). The Pohorje massif is furthermore covered by the mid-Miocene sediments of the Ribnica Trough.

During the Neogene, the Pohorje Mountains were folded into a large antiform with an ESE-NWN striking axis (Kirst et al., 2010). The central part of the Pohorje antiform is occupied by a granodioritic to tonalitic Miocene intrusion (Fodor et al., 2008; Trajanova et al., 2008). The intrusion is regarded as a batholith and is accompanied by rhyodacitic dykes and thin lamprophyre dykes in the Northwest and West of the pluton (Trajanova et al., 2008). U – Pb analyses on zircon yield an Early Miocene crystallization age of 18.64 ± 0.11 Ma, distinguishing the Pohorje pluton from the numerous Oligocene age tonalite intrusions along the Periadriatic lineament (Fodor et al., 2008).

The SBUC is located in the very South of the Pohorje Mountains and extends over 8 km from East to West with a width of roughly 1 km. This unit occupies the core of the Slovenska Bistrica Antiform which consists of a gneiss-dominated series (Kirst et al., 2010). The SBUC contains a large body of ultramafic rocks whose main protoliths are harzburgites and dunites (Hinterlechner-Ravnik et al., 1991). Extensive serpentinization left only a few garnet peridotites, garnet pyroxenites, and coronitic metatroctolites behind (Janák et al., 2006; Kirst et al., 2010). The ultramafic section furthermore includes several lenses, boudins, and bands of eclogites. Remnants of an UHP assemblage are preserved within the garnet peridotites and eclogites of the SBUC. A schematic profile of the investigated area including the described units is shown in Figure 2.

2.2 Paleogeography and Timing

The tectonic history of the southeastern Alps begins in the Permian period with LP-HT metamorphism during a rifting event (Schuster & Stüwe, 2008). This entails the metamorphism of Paleozoic and older sediments with continental and oceanic composition (Kirst et al., 2010). At that time, the Pohorje, Koralpe and Saualpe complexes were at the basement of this rift where gabbroic bodies had been emplaced within the metasediments and orthogneisses of the later Austroalpine continent (Janák et al., 2009).

The Austroalpine nappes belonged to the Apulian (Adriatic) continental plate. In the Middle Triassic the Meliata Ocean, an extension of the Neotethys Ocean, opened up to the East of Apulia. During the Late Middle and Upper Triassic, oceanic crust was produced before the Meliata Ocean started to become subducted towards the Southeast during the Jurassic. Roughly at the same time, in the Middle Jurassic, rifting more northwards led to the opening of the Piedmont-Liguria Ocean as a result of the opening of the Atlantic Ocean. After the

closure of the Meliata Ocean, convergence continued within the continent and resulted in a south- to southeast-dipping, intra-continental subduction zone (Janák et al., 2004; Stüwe & Schuster, 2010; Tenczer & Stüwe, 2003). The subduction zone formed in the northwestern foreland of the Meliata suture and possibly started along a failed Permian rift (Stüwe & Schuster, 2010). In this scenario, the Lower Central Austroalpine units, which represented the northwestern parts of the Austroalpine continental crust, were subducted under the Upper Central Austroalpine in the southeast. Consequently, the high- and ultrahigh-pressure metamorphism is restricted to the Lower Central Austroalpine units (Janák et al., 2009). The ongoing subduction led to thrusting and nappe stacking onto the northern Apulian continental block and to high- and ultrahigh-pressure metamorphism (Janák et al., 2004). The high pressures determined for these rocks indicate burial depths of up to 100 km (Janák et al., 2015).

The timing of the eclogite facies metamorphism is Cretaceous as shown by several studies. Lu – Hf garnet chronometry yields ages from 97 to 90 Ma for eclogites in the SBUC (Sandmann et al., 2016), Sm – Nd dating of garnet in metapelites resulted in ages of 93 – 87 Ma (Thöni, 2002), U – Pb zircon ages from gneisses reveal ages of 92.0 ± 0.5 Ma (Janák et al., 2009) and garnet Sm – Nd as well as zircon U – Pb dating yields ages of around 90.7 ± 3.9 Ma for eclogites (Miller et al., 2005). These values are similar to the ages of high-pressure metamorphism and cooling ages for the Koralpe and Saualpe (Thöni & Jagoutz, 1992; Thöni & Miller, 1996; Miller & Thöni, 1997; Thöni, 2002), suggesting a common tectonic history during the Eoalpine subduction and exhumation (Janák et al., 2004).

The main exhumation, which took place during the Upper Cretaceous, was most likely triggered by a slab extraction (Froitzheim et al., 2003; Tenczer & Stüwe, 2003; Janák et al., 2004, 2006). The mantle and lower crustal wedge overlying the subducted rocks was removed downwards, thus allowing these very deeply subducted rocks to be exhumed. The details of this process, however, are still unclear. The SBUC was either interpreted to have been part of the downgoing plate from the beginning (Kirst et al., 2010) or introduced from the overlying mantle wedge later on during the subduction (Janák et al., 2006). Furthermore, the Plankogel detachment and the Plattengneis shear zone of the Koralpe have been recently suggested to belong together ("PGPK shear zone" after Schorn & Stüwe, 2016) and to represent the suture of this subduction zone (Schorn & Stüwe, 2016).

During the Paleocene and Eocene, the collision of the Apulian and European continent emplaced the Austroalpine nappe stack towards the North on top of the Penninic units (derived from the Penninic ocean) and Helvetic units (derived from the European continental margin) (Janák et al., 2004). The final exhumation to the surface occurred through east- to north-east-directed low-angle extensional shearing during the Early to Middle Miocene. This is shown by apatite and zircon fission track ages of 19 – 10 Ma and K – Ar mica ages of 19 – 13 Ma from country rocks of eclogites and metaultrabasites (Fodor et al., 2002).

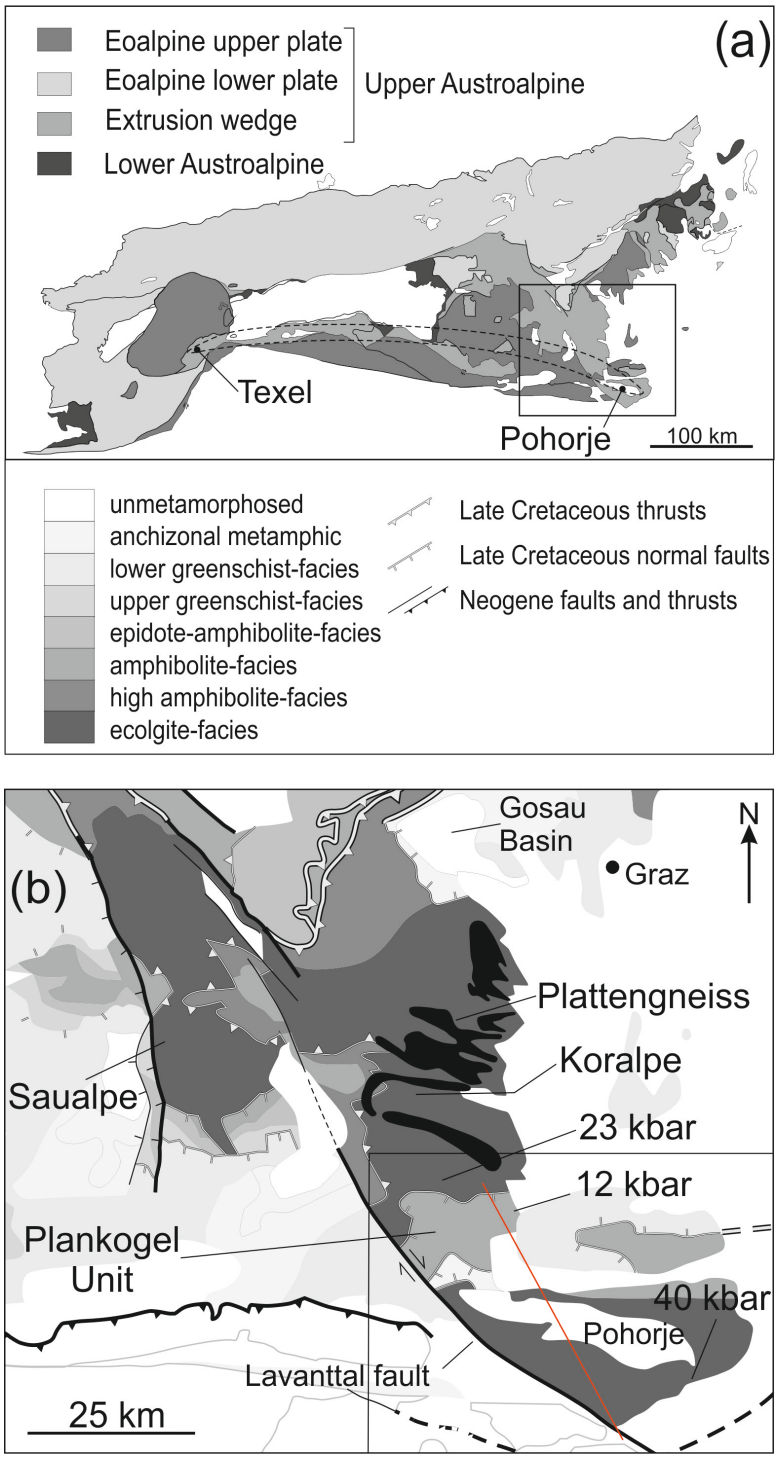

Figure 1: (a) Simplified geological map of the Eastern Alps (modified after Schmid et al., 2004). The dotted line indicates the Eoalpine high pressure belt from the Texel Complex to the Pohorje Mountains. (b) Simplified geological map of the Saualpe-Koralpe-Pohorje area showing major structures (modified after Froitzheim et al., 2008). Indicated pressures are according to Schorn & Stüwe (2016) and Janák et al. (2006). The red line indicates the transect along which samples were taken. The box matches to the zoom-in shown in Fig. 2.

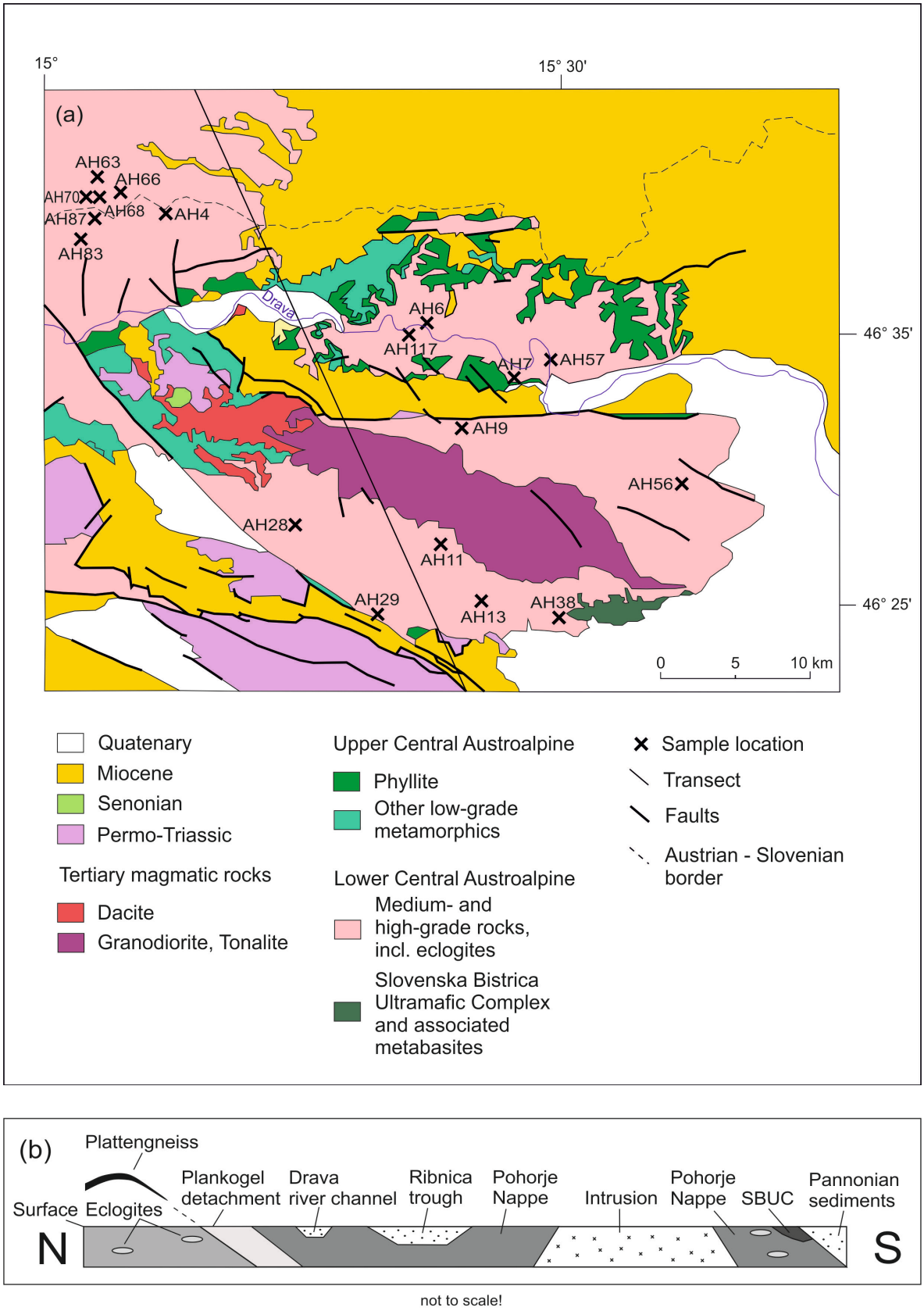

Figure 2: (a) Simplified geological map showing the investigated area (modified after Mioč & Žnidarčič, 1977). The black line represents the transect along which samples were projected. Sample localities are marked within the map. (b) North to South simplified cartoon section through the research area roughly along the transect line shown in (a) (modified after Schorn & Stüwe, 2016).

3 PETROGRAPHY AND MINERAL CHEMISTRY

For the purpose of this thesis around 120 samples were collected in the area of the transect line shown in Figure 1 & 2. The study area is mostly wooded and sparsely populated. Relatively unaltered material and outcrops can mainly be found along forest roads and main roads. The sample locations were selected exclusively from the Pohorje Nappe and metapelites of the southern Koralpe. Samples from the SBUC unit were also taken but not further analyzed since they are not the focus of this study. The ultramafic rocks have already been described in detail above in the geological description of the study area.

The metapelitic samples were carefully sorted out and 43 thin-sections were made. Amphiboles, eclogites, strongly weathered samples, and samples which appeared to have a lack of petrologically useful phases were neglected. The remaining sample locations and coordinates are shown in Figure 2 and Appendix 1, respectively. Photographs of representative thin-sections are shown in Figures 3 & 5.

The thin-sections were analyzed under a polarizing microscope and 20 samples were chosen for further analyses with the electron microscope and geothermobarometric calculations. For each thin-section several spots suitable for analyses were selected and marked. Minerals in close vicinity of each other were measured in order to be able to constrain the metamorphic conditions of each sample.

Mineral chemical analyses were carried out using a JEOL JSM-6310 scanning electron microscope equipped with a Link ISIS EDX-System and Microspec WDX-600i system at the Institute of Earth Sciences, University of Graz, Austria. Measurements were performed on polished, carbon-coated thin-sections with measurement conditions of 15 kV acceleration voltage and 6 nA beam current. Representative mineral analyses are shown in Tables 3, 4 & 5. Mineral abbreviations are according to THERMOCALC.

3.1 Koralpe

The Koralpe consists of a polymetamorphic sequence containing micaschists and pelitic gneisses (appearing as the so-called ultramylonitic Plattengneis shear zone), including lenses of metagabbros, eclogites, marbles, amphibolites and pegmatitic veins (Thöni & Jagoutz, 1992; Gregurek et al., 1997; Miller & Thöni, 1997). Samples were not taken from this area, however, the petrology of the Koralpe Complex is briefly described.

The pelitic rocks are divided into micaschists and gneisses. The typical assemblage for micaschists includes garnet, muscovite, biotite, plagioclase and quartz, whereas the gneiss assemblage commonly contains garnet, muscovite, biotite, plagioclase, potassium feldspar, quartz and kyanite (Tenczer & Stüwe, 2003). All pelitic rocks are typically foliated and exhibit medium grain sizes (Miller & Thöni, 1997). Garnet porphyroblasts are rich in inclusions and present in all assemblages of the pelitic rocks (Gregurek et al., 1997; Tenczer & Stüwe, 2003). White mica as well as kyanite, staurolite and plagioclase are common in micaschists (Tenczer & Stüwe, 2003).

Feldspar porphyroblasts are typical for the Plattengneis type rocks. Feldspars are highly strained and show textures of dynamic recrystallization (Tenczer & Stüwe, 2003). Quartz forms either layers or occurs as lenses with rather uniform grain sizes in the Plattengneis type rocks, whereas the irregular grain size distribution within different layers is caused by the occurrence of plagioclase, white mica and biotite (Kurz et al., 2002). Garnets within the gneisses are partly boudinaged and often surrounded by biotite (Kurz et al., 2002). Kyanite occurs commonly as elongated aggregates (Tenczer & Stüwe, 2003).

3.2 Plankogel Unit

The Plankogel Unit is characterized by a sequence of garnet-micaschists, thin layers of manganese quartzite and lenses of metaultrabasites and metabasites (Kleinschmidt, 1975). Samples were taken exclusively from the micaschists. Garnet-micaschists from the Plankogel Unit show a fine to medium grained matrix with larger garnet porphyroblasts. The matrix is made up of quartz, muscovite and biotite.

Quartz makes up over 50 percent of the modal abundances within the thin-sections. Most grains do not differ much in grain size and show undulose extinction. Garnets from the Plankogel Unit form relatively large porphyroblasts with diameters of up to 1 cm. Most of them also exhibit some sort of compositional or textural zoning as shown in Figure 4. Zoned garnets exhibit a slight decrease in MgO and CaO and an increase of FeO towards the core. Representative mineral analyses of a zoned garnet are shown in Appendix 5. Inclusions of quartz, biotite, muscovite, chlorite, chloritoide and staurolite occasionally occur within garnets.

Muscovite can be found throughout all thin-sections occurring either as mica fish, as smaller grains distributed within the matrix or as inclusion in garnets. In some samples it is characterized by very small grains making up a fine matrix. Biotite occurs in most samples as fine grains within the matrix or as inclusions in garnet. It also occurs in association with chlorite on the outside of larger garnet grains.

Plagioclase is only present in small amounts in sample AH4. Small grains of plagioclase showing typical twin lamellae can be found within the quartz-dominated matrix. Staurolite is common in most samples of the Plankogel Unit. It appears in several thin-sections in the shape of subhedral elongated grains with up to 3 mm in length. They were found within the matrix or as inclusions within a garnet. Zoisite was found only in sample AH4 in the shape of needles following the orientation of the foliation.

Chloritoide occurs only in samples AH87 and AH83 either as inclusion within a garnet or in the matrix. Minerals are euhedral and relatively big with a length of up to almost 1 mm. Chlorite is present in most samples within the matrix or as inclusion in garnets. Most of the time it appears to be of secondary nature. Kyanite is only found in sample AH63 as small grains within the matrix. Accessories are mostly rutile, epidote and opaque phases such as ilmenite.

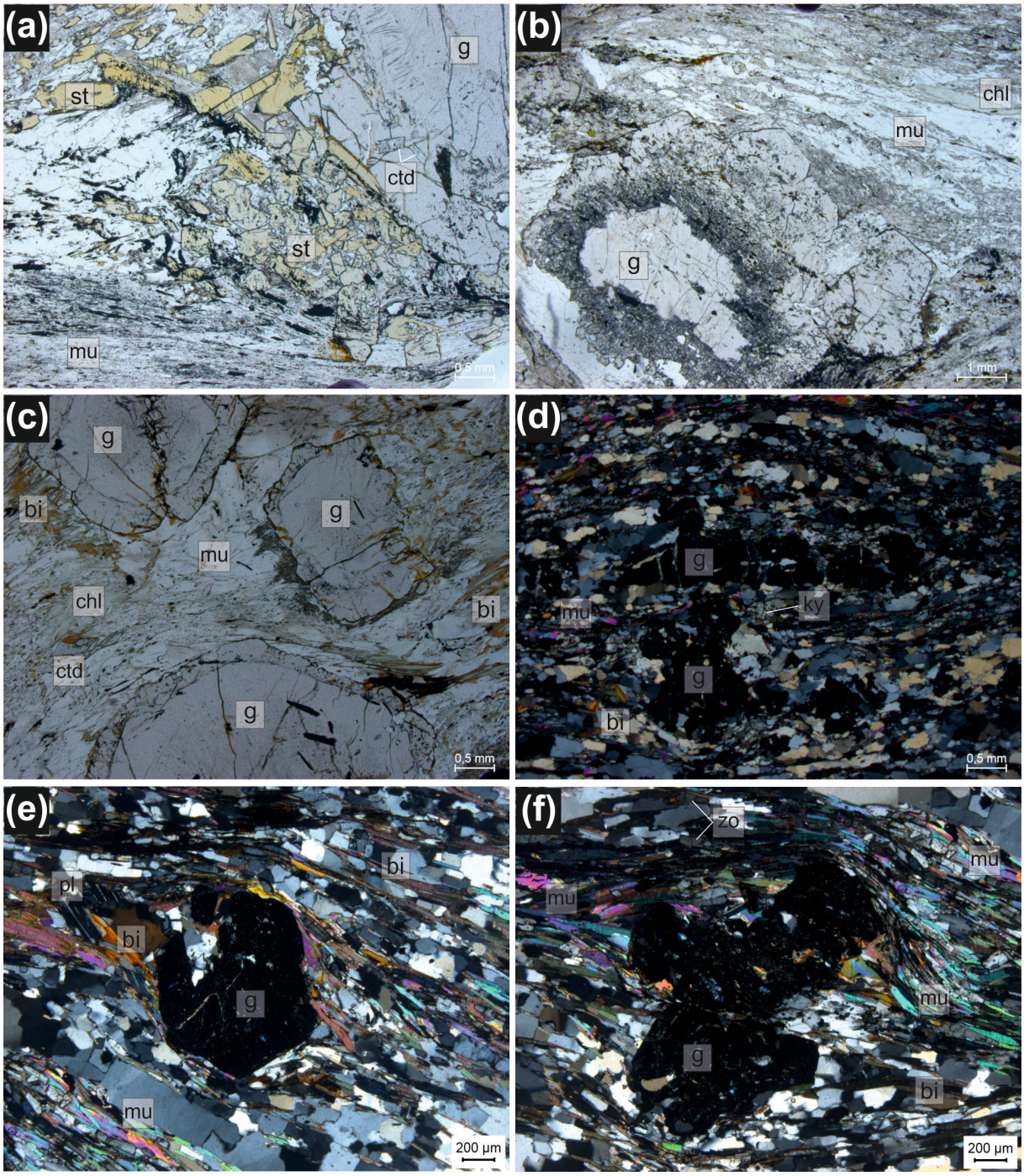

Figure 3: Photomicrographs of representative samples taken from the Plankogel Unit. (a)-(c) are shown under parallel polarizing filters and (d)-(f) are shown under crossed polarizing filters. (a) Sample AH87: Garnet-micaschist displaying a zoned garnet porphyroblast with inclusions of chloritoide and staurolite. The matrix is characterized by fine-grained muscovite and quartz including a lot of staurolite. (b) Sample AH68: Large garnet porphyroblast with visible zoning within a matrix of muscovite, quartz and secondary chlorite. (c) Sample AH83: Several garnet porphyroblasts exhibiting visual zoning within a matrix of muscovite, quartz, biotite and secondary chlorite. (d) Sample AH70: Several garnets within a matrix of quartz, muscovite and biotite. Note the kyanite in between the garnet grains. (e) & (f) Sample AH4: Garnet-micaschist showing several garnet prophyroblasts. (e) shows a plagioclase next to the garnet whereas (f) displays several needles of zoisite alongside muscovite surrounding the garnet.

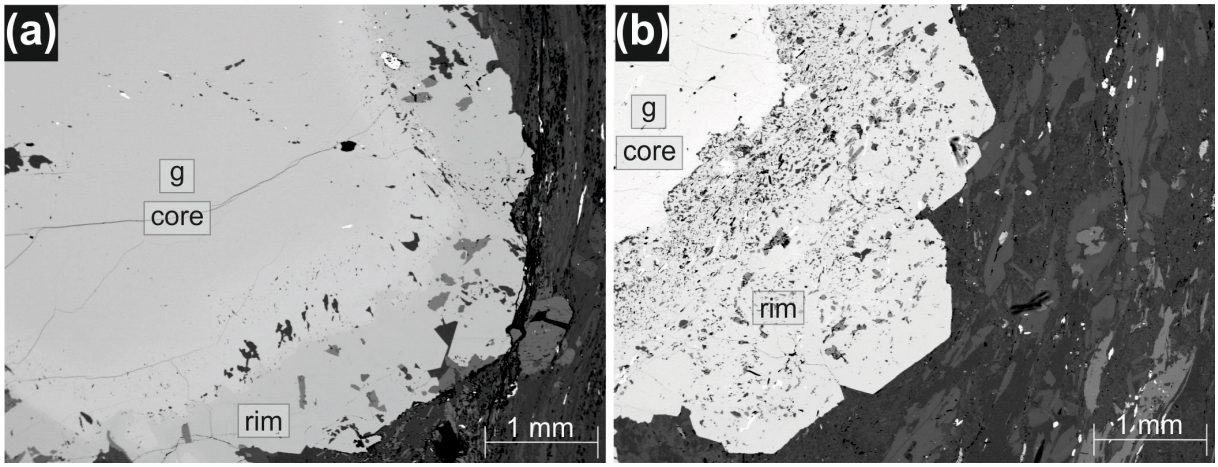

Figure 4: Large garnet porphyroblasts viewed under the electrone micrsocope. Different shading represents different chemical compositions. A separate core and rim can be viewed in both images. (a) Sample AH87 and (b) Sample AH68 were both taken from the garnet-micaschists of the Plankogel Unit.

3.3 Pohorje Nappe

The metapelites of the Pohorje Nappe are mainly coarse-grained gneisses and micaschists with similar mineral assemblage. They are commonly foliated and show a general composition of quartz + garnet + muscovite + biotite ± plagioclase ± staurolite ± zoisite ± chloritoide ± chlorite ± kyanite. Samples in the Pohorje Mountains show a fine to medium grained matrix. The matrix generally consists of quartz, muscovite and biotite.

Quartz makes up over 50 percent of the modal abundances within all thin-sections in the Pohorje Nappe. Quartz grains show undulose extinction, and grain boundary migration, indicating temperature conditions of around 600 °C. They do not differ much in grain size and are generally quite similar to the Plankogel Unit. Garnet grains are mostly subhedral and slightly fractured. Samples in the Pohorje Nappe include significantly smaller specimen than in the North with not so obvious visible or compositional zoning. Inclusions of quartz, biotite, muscovite and chlorite occasionally occur within the garnets.

Muscovite can be found throughout all thin-sections in varying quantity. Muscovites occur either as big mica fish, as smaller grains distributed within the matrix or as inclusion in garnets. Mineral analyses show various compositions for muscovites in different samples. Mineral analyses can be compared in Appendix 3 & 4 and in Tables 3, 4 & 5. Biotite occurs in most samples as subhedral elongated grains within the matrix or as inclusions in garnet.

Plagioclase was only found in some thin-sections and always in relatively small amounts within the matrix. Grains are subhedral to anhedral and typically show twin lamellae. Staurolite appears occasionally as very small grains within the matrix. Staurolite is quite rare in samples collected from the Pohorje Mountains, however, it is pretty common in samples collected from the Plankogel Unit.

Chlorite is found in most samples within the matrix or as inclusion in garnets. Chlorite also occasionally appears to be of secondary nature, for example, on the edge of biotite grains. Kyanite is only sporadically present within the examined thin-sections and can be found as small grains within the matrix in samples AH29 and AH56. Accessories are mostly rutile, epidote and opaque phases such as ilmenite.

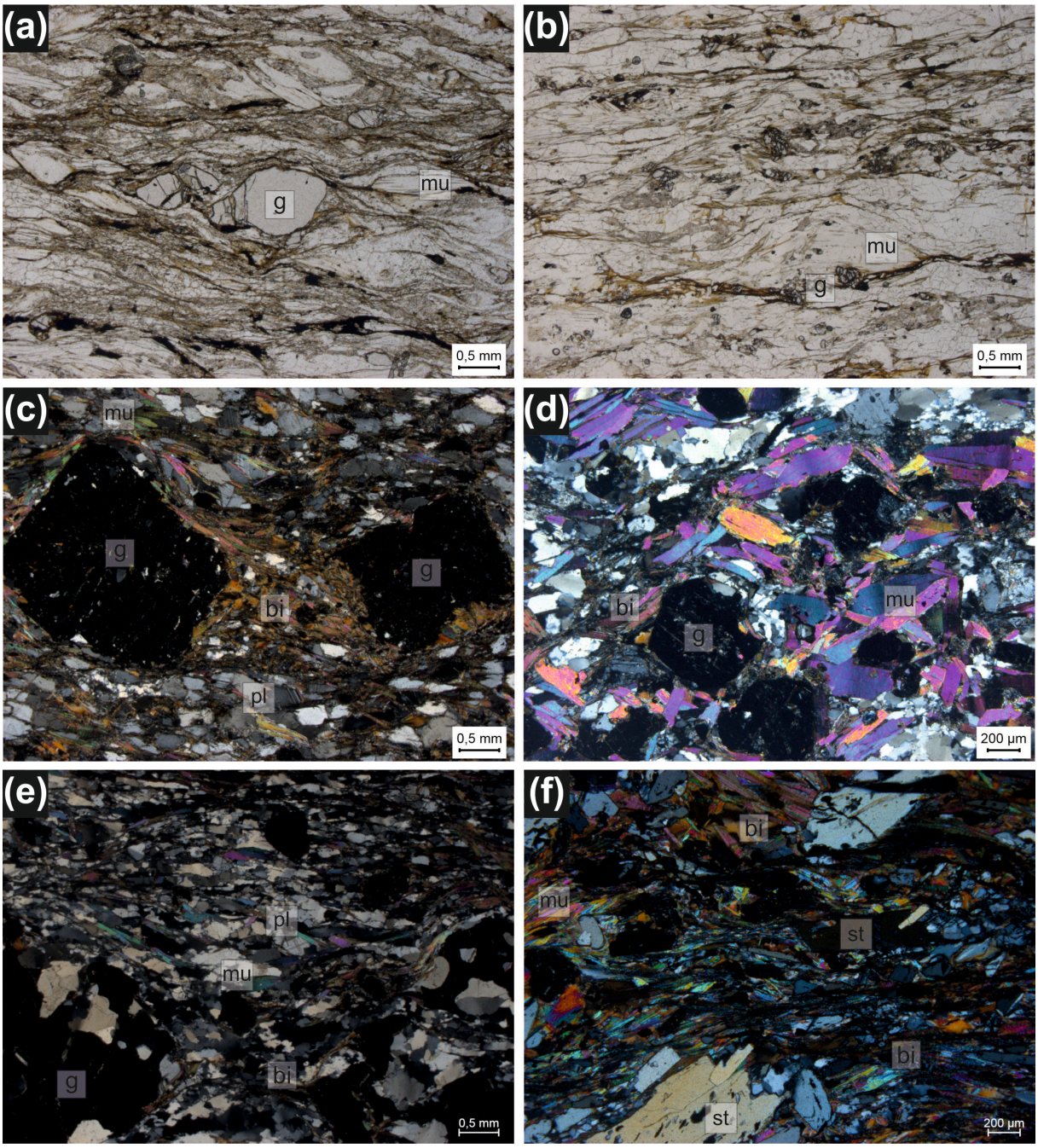

Figure 5: Photomicrographs of representative samples taken from the Pohorje Nappe. (a) & (b) are shown under parallel polarizing filters and (c)-(f) are shown under crossed polarizing filters. (a) Sample AH11: Small garnet porphyroblasts within a matrix of mainly quartz. Large mica fish are present within the thin-section. (b) Sample AH 13: Garnet is only sporadically present within a matrix of quartz and muscovite. (c) Sample AH6: Large garnet porphyroblasts within a matrix of quartz, biotite and muscovite which also occasionally displays plagioclase. (d) Sample AH7: Garnets and large mica fish are found within a matrix of quartz. (e) Sample AH29: Fine-grained matrix includes garnet porphyroblasts and sporadic plagioclase. (f) Sample AH56: Fine-grained matrix of mainly muscovite and biotite contains small garnet and large staurolite porphyroblasts.

4 GEOTHERMOBAROMETRY

The mineral analyses from the electron microscope were used for pressure and temperature calculations. Geothermobarometry was performed using THERMOCALC version 3.33 (http://www.metamorph.geo.uni-mainz.de/thermocalc/software/index.html; Powell & Holland, 1988). THERMOCALC is a program for thermodynamic calculations utilizing an internally-consistent thermodynamic dataset (Holland & Powell, 1998). Calculations were performed with the average *P-T* method, as well as the average *P* method of Powell & Holland (1994).

A mineral assemblage that is interpreted to have once been in equilibrium is chosen and end-members of the minerals for which there is data in the dataset are entered into the program. THERMOCALC calculates a set of independent reactions and combines them in order to calculate the conditions of formation for the desired mineral assemblage.

Temperatures were constrained by average *PT* calculations, as well as by existing information from published papers (e.g. Janák et al., 2004, 2009, 2015; Hurai et al., 2009). The average *P* method was used to calculate pressure values for a defined temperature from the set of equilibrium relations.

Chemical compositions of minerals in close vicinity of each other were entered in the AX program (http://www.esc.cam.ac.uk/research/research-groups/research-projects/tim-hollands-software-pages/ax) in order to obtain end-member activities. AX generates several output files including a simple text file of end-members and their activities which is furthermore used to undertake THERMOCALC calculations. Water has been assumed to be in excess in all samples since they are rich in hydrous equilibrium phases and thus H_2O has been added into the input file. THERMOCALC mode 2 (average *P-T* calculations) and rock calculations type 1 (average *P*) are entered into the program. After confirming the data and setting either a temperature window or a fixed temperature, pressure values are calculated for the desired conditions. The output shows a pressure result with a corresponding error margin and sigfit value. The sigfit value shows the quality of how well selected end-member activities match among one another. The smaller the sigfit value the more accurate and reliable the result is going to be. Different combinations of mineral analyses were tested for each individual sample in order to keep the error margin and sigfit values as low as possible and achieve reliable results.

At first, geothermobarometry was carried out with the mineral assemblage at hand for each sample. The assemblages and reactions determined for each thin-section are reported in Appendix 2 and vary slightly amongst different samples.

Using the whole assemblage, calculations yielded pressure values in the range of 7.1 – 12.9 kbar which seems to be relatively low considering the geological setting. Janák et al. (2009) performed similar calculations for metapelites in the immediate surroundings of the SBUC and argued that these values represent the decompression conditions and not the desired peak metamorphic conditions. They furthermore calculated the peak conditions by using only garnet cores + phengite + kyanite + quartz. This method yielded significantly higher pressures which are, however, still considered as minima due to the possibility of diffusion-related modification of the garnet composition at high temperatures and the re-equilibration of phengite during early stages of decompression (Janák et al., 2009).

Considering this idea, peak metamorphic conditions were worked out using only the suggested assemblage of g + mu + ky + qu. Kyanite is only present in a few thin-sections but was assumed to be abundant throughout all samples in order to simplify pressure calculations with THERMOCALC.

The error margin increased due to the smaller amounts of data entered into the program, however, sigfit values decreased, showing well-corresponding data. The obtained pressures show significantly higher values than the previous calculations, even despite their higher error margin. The results for both methods are presented in Figure 6 and Tables 1 & 2. Detailed chemical analyses are shown in Tables 3, 4 & 5 and in Appendix 3 & 4.

For samples from the Plankogel Unit (AH4, AH63, AH68, AH66, AH70, AH83& AH87) yet another approach had to be used. As mentioned in the detailed geological description, the Plankogel Unit, as opposed to the Pohorje Nappe, still preserves relics of the Permian metamorphic event in its garnet cores (Thöni & Miller, 2009; Janák et al., 2009, 2015). The method used for determining pressures in the Pohorje Nappe is thus useless for this part of the research area. Measurements of Permian garnet cores combined with measurements of micas of the Cretaceous assemblage would only yield wrong pressure values. Therefore, pressures for the Plankogel Unit were determined by using chemical data from the garnet rims and the rest of the assemblage. It can be assumed that these values correspond well to the Cretaceous conditions, since the Plankogel Unit does not exhibit further signs of other significant

compositional changes. Hence, these values can be compared with the pressure values from the Pohorje Nappe, even though a different method was used to obtain them.

Furthermore, it should be noted that pressure determinations are prone to large uncertainties which unfortunately complicate any interpretation. Inaccuracies can stem from lacking analytical precision and geological precision or from mistakes in the thermodynamic data and activity-composition models. Different methods were tried in order to achieve more accurate pressure values.

The del-*PT* method, for example, attempts to decrease the error margin by directly comparing the end-member activities of two different samples, thus, eliminating any errors stemming from analytical data. In the case of this study the del-*PT* method, however, could not be used since it always requires the same mineral assemblage for all samples. Theoretically, this would work for the peak metamorphic assemblage of gr + ph + ky + qu but the calculations only resulted in even higher uncertainties since these pressures were quite imprecise to begin with.

The best method to achieve pressure values as accurate as possible proved to be simply to change temperature conditions within THERMOCALC and to repeatedly replace individual measurements of the same mineral with each other. For the re-equilibrated conditions it worked best to use measurements of minerals in close proximity to each other.

In order to be able to compare the obtained pressure values, the temperature has been set to 700 °C for the peak metamorphic conditions and to 650 °C for the retrograde metamorphic conditions and the samples from the Plankogel Unit. Some samples did not yield any results by using the assemblage of g + mu + ky + q which explains the smaller amount of results for peak metamorphic conditions.

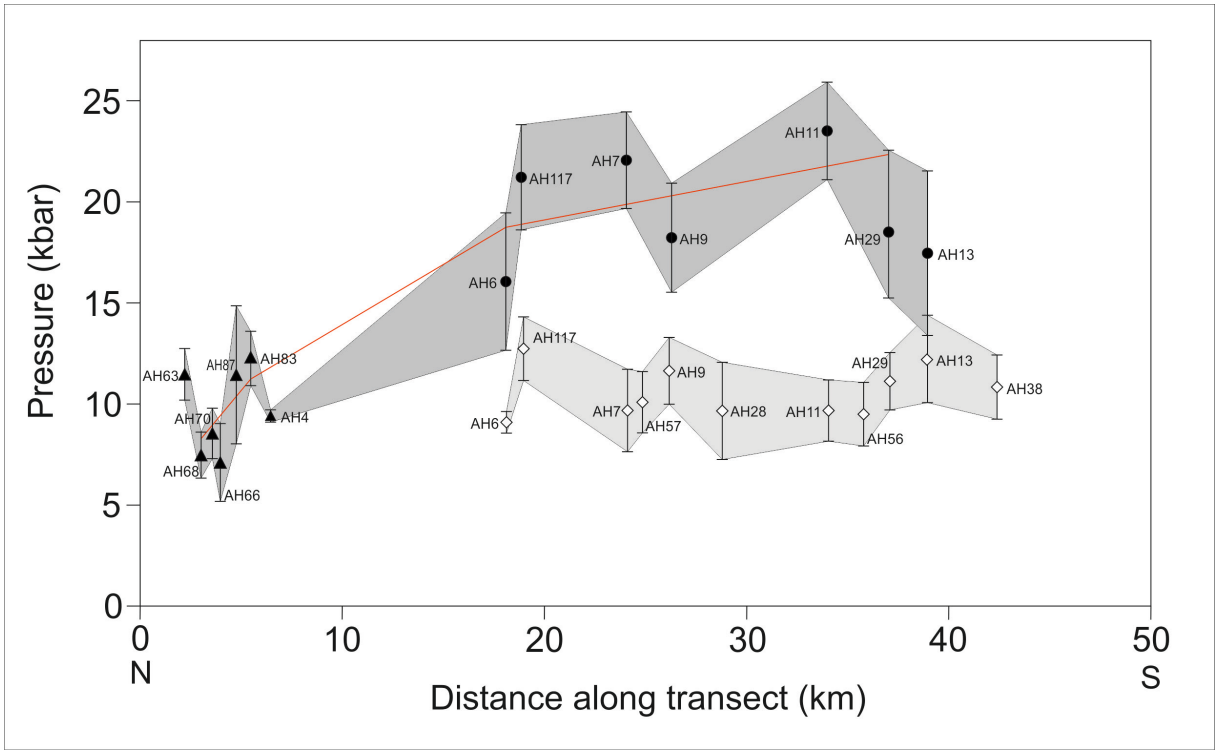

Figure 6: Visual representation of pressure results determined with THERMOCALC. The black triangles represent the Plankogel Unit, the black circles represent the peak metamorphic conditions of the Pohorje Nappe and the white squares represent the decompression conditions of the Pohorje Nappe. The transect starts in the North with the beginning of the Plankogel Unit and ends in the South where the Pohorje Mountains dip below the sediments of the Pannonian Basin. The darker shaded area shows the rising pressures from North to South and the lighter shaded area represents the re-equilibrated pressures. The red line visually represents the interpreted gradient discussed in Chapter 6.

Table 1: Results of *P* calculations at 650°C

Sample	*P* (kbar)	sd (kbar)	sigfit	Sample	*P* (kbar)	sd (kbar)	sigfit
AH68	7.5	1.11	1.0	AH9	11.7	1.73	1.3
AH70	8.8	1.21	0.9	AH28	9.7	2.54	0.8
AH66	7.1	1.95	0.8	AH11	9.8	1.60	2.7
AH87	11.5	3.42	2.8	AH29	11.2	1.42	1.0
AH83	12.5	1.29	1.9	AH56	9.6	1.80	0.9
AH4	9.4	0.23	0.4	AH13	12.3	2.25	1.3
AH117	12.9	1.83	2.0	AH38	10.9	1.70	1.0
AH6	9.1	0.56	0.7	AH63	11.5	1.36	1.0
AH7	9.7	2.00	3.7	AH57	10.1	1.55	2.9

Table 2: Results of *P* calculations with the assemblage g + mu + ky + q at 700°C

Sample	*P* (kbar)	sd (kbar)	sigfit
AH6	16.2	3.45	1.0
AH117	21.3	2.72	1.2
AH7	22.2	2.38	0.1
AH9	18.1	2.84	0.9
AH11	23.9	2.49	0.1
AH29	18.6	3.58	1.1
AH13	17.5	4.06	1.3

Table 3: Representative mineral compositions for metapelite samples AH7 and AH11

Sample	AH7	AH11	AH7	AH11	AH7	AH11	AH7	AH11	AH7	AH11
Phase	Garnet		Muscovite		Biotite		Chlorite		Feldspar	
Position	rim	rim	matrix	matrix	matrix	matrix	matrix	matrix	matrix	matrix
Label	ah7_1_11	ah11_2_1	ah7_1_17	ah11_1_25	ah7_1_18	ah11_5_18	ah7_2_7	ah11_7_10	ah7_4_2	ah11_7_6
SiO_2	38.33	37.58	48.08	47.99	36.43	34.53	25.87	25.12	64.88	38.94
TiO_2	0.01	0.00	1.09	0.91	1.71	1.58	0.05	0.04	0.07	0.06
Al_2O_3	21.31	20.73	32.32	31.38	16.64	17.33	20.40	20.92	23.39	31.64
Cr_2O_3	0.10	0.04	0.06	0.06	0.09	0.02	0.04	0.00	0.01	0.08
Fe_2O_3	1.60	1.31	0.00	0.00	0.00	1.83	0.00	0.00	0.00	1.13
FeO	25.70	24.78	1.68	1.60	18.73	17.89	29.82	24.38	0.00	0.00
MnO	0.63	0.49	0.00	0.01	0.12	0.16	0.24	0.32	0.00	0.09
MgO	3.99	5.52	1.83	2.17	10.87	10.26	11.55	15.22	0.00	0.07
CaO	9.54	7.55	0.00	0.00	0.04	0.08	0.06	0.02	4.27	23.02
Na_2O	0.04	0.03	0.81	0.65	0.09	0.14	0.00	0.03	9.31	0.08
K_2O	0.00	0.00	10.32	9.60	9.55	8.45	0.05	0.00	0.11	0.03
Total	101.24	98.04	96.20	94.37	94.27	92.29	88.09	86.06	102.03	95.13
Oxygen	12.0	12.0	11.0	11.0	11.0	11.0	14.0	14.0	8.0	8.0
Si	2.977	2.990	3.176	3.214	2.800	2.709	2.777	2.690	2.807	1.944
Ti	0.000	0.000	0.054	0.046	0.099	0.093	0.004	0.004	0.002	0.002
Al	1.951	1.944	2.517	2.478	1.508	1.603	2.582	2.642	1.193	1.862
Cr	0.006	0.003	0.003	0.003	0.005	0.001	0.004	0.000	0.000	0.003
Fe^{3+}	0.094	0.079	0.000	0.000	0.000	0.108	0.000	0.000	0.000	0.042
Fe^{2+}	1.669	1.649	0.093	0.090	1.204	1.174	2.677	2.184	0.000	0.000
Mn	0.041	0.033	0.000	0.000	0.008	0.011	0.021	0.029	0.000	0.004
Mg	0.462	0.655	0.180	0.216	1.245	1.200	1.847	2.429	0.000	0.005
Ca	0.794	0.643	0.000	0.000	0.003	0.007	0.007	0.003	0.198	1.231
Na	0.006	0.005	0.104	0.085	0.013	0.022	0.000	0.007	0.781	0.008
K	0.000	0.000	0.870	0.820	0.936	0.846	0.007	0.000	0.006	0.002
Total	8.000	8.000	6.997	6.953	7.821	7.776	9.929	9.988	4.987	5.104

Table 4: Representative mineral compositions for metapelite samples AH83 and AH87

Sample	AH83	AH87	AH83	AH87	AH83	AH87	AH83	AH87	AH83	AH87	AH83	AH87
Phase	Garnet		Muscovite		Biotite		Chlorite		Staurolite		Chloritoid	
Position	rim	rim	matrix	matrix	matrix	matrix	matrix	matrix	matrix	matrix	matrix	matrix
Label	ah83_12_22	ah87_42_3	ah83_12_3	ah87_21_7	ah83_12_6	ah87_21_3	ah83_11_7	ah87_21_5	ah83_12_18	ah87_21_35	ah83_12_9	ah87_21_15
SiO_2	37.88	36.97	48.78	47.07	37.23	26.56	26.66	26.07	28.57	28.62	25.31	24.38
TiO_2	0.01	0.02	0.39	0.36	1.41	0.13	0.15	0.10	0.38	0.58	0.01	0.03
Al_2O_3	21.11	21.25	38.21	35.75	20.03	23.96	24.01	24.33	56.72	53.02	42.67	40.01
Cr_2O_3	0.06	0.00	0.03	0.01	0.00	0.12	0.00	0.02	0.04	0.00	0.00	0.00
Fe_2O_3	0.00	1.11	0.00	0.00	0.00	3.87	0.00	0.00	0.00	0.00	0.00	0.00
FeO	37.08	30.93	0.96	0.93	19.59	19.71	24.64	22.61	14.54	14.18	23.38	21.35
MnO	0.73	0.04	0.01	0.00	0.02	0.00	0.00	0.00	0.03	0.05	0.09	0.00
MgO	1.93	3.49	0.27	0.37	10.52	17.84	14.23	18.25	2.01	2.27	3.20	4.12
CaO	2.15	5.42	0.01	0.00	0.01	0.00	0.03	0.00	0.02	0.03	0.00	0.00
Na_2O	0.00	0.00	1.87	1.78	0.29	0.00	0.03	0.02	0.00	0.00	0.00	0.00
K_2O	0.04	0.03	8.62	8.75	9.07	0.03	0.25	0.02	0.03	0.00	0.03	0.00
Total	100.99	99.26	99.15	95.01	98.18	92.22	90.02	91.41	102.34	98.75	94.70	89.89
Oxygen	12.0	12.0	11.0	11.0	11.0	11.0	14.0	14.0	46.0	46.0	6.0	6.0
Si	3.030	2.963	3.079	3.109	2.727	2.039	2.704	2.580	7.584	7.875	1.009	1.019
Ti	0.001	0.001	0.019	0.018	0.078	0.008	0.012	0.007	0.075	0.120	0.000	0.001
Al	1.991	2.008	2.843	2.784	1.730	2.168	2.871	2.838	17.750	17.198	2.005	1.971
Cr	0.004	0.000	0.001	0.001	0.000	0.007	0.000	0.002	0.009	0.000	0.000	0.000
Fe^{3+}	0.000	0.067	0.000	0.000	0.000	0.223	0.000	0.000	0.000	0.000	0.000	0.000
Fe^{2+}	2.481	2.073	0.051	0.051	1.200	1.265	2.090	1.871	3.228	3.262	0.779	0.746
Mn	0.050	0.003	0.001	0.000	0.001	0.000	0.000	0.000	0.008	0.012	0.003	0.000
Mg	0.230	0.417	0.025	0.037	1.148	2.041	2.151	2.691	0.794	0.930	0.190	0.257
Ca	0.184	0.465	0.001	0.000	0.001	0.000	0.003	0.000	0.006	0.007	0.000	0.000
Na	0.000	0.000	0.228	0.228	0.041	0.000	0.006	0.003	0.000	0.002	0.000	0.000
K	0.004	0.003	0.694	0.737	0.848	0.003	0.033	0.003	0.010	0.000	0.002	0.000
Total	7.974	8.000	6.942	6.964	7.775	7.755	9.869	9.996	29.466	29.407	3.989	3.994

Table 5: Representative mineral compositions for UHP calculations of samples AH117, AH7, AH9 & AH11

Sample	AH117	AH7	AH9	AH11	AH117	AH7	AH9	AH11
Phase	Garnet				Muscovite			
Position	core	core	core	core	matrix	matrix	matrix	matrix
Label	ah117_2_9	ah7_1_3	ah9_3_9	ah11_5_9	ah117_2_12	ah7_2_9	ah9_1_5	ah11_1_24
SiO_2	37.17	38.22	36.99	37.44	46.72	48.70	46.04	49.32
TiO_2	0.10	0.00	0.06	0.08	0.65	0.66	1.45	0.88
Al_2O_3	20.67	21.13	20.28	20.71	34.48	32.14	33.42	30.77
Cr_2O_3	0.02	0.03	0.00	0.01	0.03	0.00	0.05	0.14
Fe_2O_3	3.18	1.86	1.64	1.55	0.00	0.00	0.00	0.00
FeO	31.29	27.59	29.26	23.31	0.91	1.69	1.50	1.61
MnO	0.41	0.92	7.52	0.71	0.00	0.00	0.00	0.00
MgO	5.23	2.69	2.79	5.22	0.53	1.84	1.34	2.45
CaO	2.70	9.37	1.67	8.95	0.03	0.02	0.04	0.00
Na_2O	0.00	0.05	0.01	0.01	1.97	0.66	0.46	0.73
K_2O	0.02	0.04	0.09	0.00	8.62	10.62	10.72	9.54
Total	100.78	101.91	100.31	97.97	93.95	96.33	95.03	95.44
Oxygen	12.0	12.0	12.0	12.0	11.0	11.0	11.0	11.0
Si	2.937	2.979	2.986	2.978	3.125	3.211	3.088	3.261
Ti	0.006	0.000	0.003	0.005	0.033	0.033	0.073	0.044
Al	1.925	1.942	1.930	1.942	2.719	2.498	2.643	2.399
Cr	0.001	0.002	0.000	0.001	0.002	0.000	0.003	0.007
Fe^{3+}	0.189	0.109	0.100	0.093	0.000	0.000	0.000	0.000
Fe^{2+}	2.068	1.799	1.976	1.551	0.051	0.093	0.084	0.089
Mn	0.027	0.061	0.514	0.048	0.000	0.000	0.000	0.000
Mg	0.615	0.313	0.336	0.619	0.053	0.181	0.134	0.242
Ca	0.229	0.783	0.144	0.763	0.002	0.001	0.003	0.000
Na	0.000	0.008	0.001	0.001	0.255	0.084	0.059	0.093
K	0.002	0.004	0.009	0.000	0.735	0.894	0.917	0.805
Total	8.000	8.000	8.000	8.000	6.977	6.997	7.005	6.941

5 PSEUDOSECTION

In order to better illustrate the mineral assemblage of a representative sample a *P-T* pseudosection was created. Sample AH29 was chosen and a bulk composition was calculated. Since mineral analyses were already obtained with the electron microscope, there was no need for XRF measurements. The bulk composition was determined by figuring out the modal abundances for each mineral with the help of the point-count method. The modal abundances are represented in Table 7. The next step simply was to multiply the modal abundances with an average mineral analysis for every oxide of every single mineral. The oxide values then had to be added up resulting in the correct bulk composition for this sample. The determined bulk composition is shown in Table 6.

Since peak pressure conditions cannot be achieved by conventional thermobarometry, equilibrium phase modeling can help to understand mineral assemblages for different pressure and temperature conditions. The pseudosection was created using THERMOCALC version 3.33 with calculation mode 1 for phase diagram calculations. Modeling was carried out in the Na2O–CaO–K2O–FeO–MgO–Al2O3–SiO2–H2O (NCKFMASH) – system. The mineral assemblage observed in thin-section AH29 contains garnet, biotite, muscovite, plagioclase, kyanite, and quartz. H_2O, muscovite and quartz were assumed to be in excess. The finished pseudosection is shown in Figure 7.

Table 6: Bulk composition in mol. % used in phase diagram modeling for sample AH29

Sample	SiO2	Al2O3	CaO	MgO	FeO	K2O	Na2O
AH29	78.555	9.176	0.531	2.593	6.645	2.450	0.051

Table 7: Modal abundances of minerals present in thinsection AH29

Mineral	Quartz	Garnet	Musovite	Biotite	Kyanite	Plagioklase
Percent	61.526	10.059	11.819	15.591	0.251	0.754

The pseudosection shows fields of different stable phase assemblages and different variance. The variance is represented by the varying shadings of the stability fields. A lighter color indicates a lower variance and a darker color indicates a higher variance, respectively.

Sample AH29 is a metapelite with noticeably low Na_2O content. This can be explained by the lack of phases containing Na_2O, in particular, by a very small amount of plagioclase within the thin-section. The low Na_2O content is representative for most other samples since plagioclase and other feldspars are very rare and occasionally not present at all. Due to the low Na_2O content muscovite is stable everywhere except for the LP/HT part of the diagram. Paragonite is never stable in the *P-T* field of this diagram. It is, however, expected to enter the diagram in a higher *P-T* field corresponding to the eclogite facies.

The stability fields lying below 500 °C are metastable towards epidote or albite and would also include titanite and rutile in a component system including TiO_2 and Fe^{3+}. Above 10 kbar several big fields are stable. Within the eclogite facies paragonite and ultimately jadeite would be added into the stability assemblage.

The pseudosection for this sample only shows the lower metamorphic conditions achieved during equilibration and not during peak metamorphism. It roughly represents the mineral assemblages which were previously used for pressure calculations with THERMOCALC. With decreasing pressures during the first stage of exhumation, the rocks reached conditions represented in this pseudosection and equilibrated to these assemblages. Remnants of prior conditions can only be seen in some minerals, such as garnets and phengites. These minerals did not fully equilibrate to the lower pressure and temperature environment and have been thus used for peak metamorphic calculations.

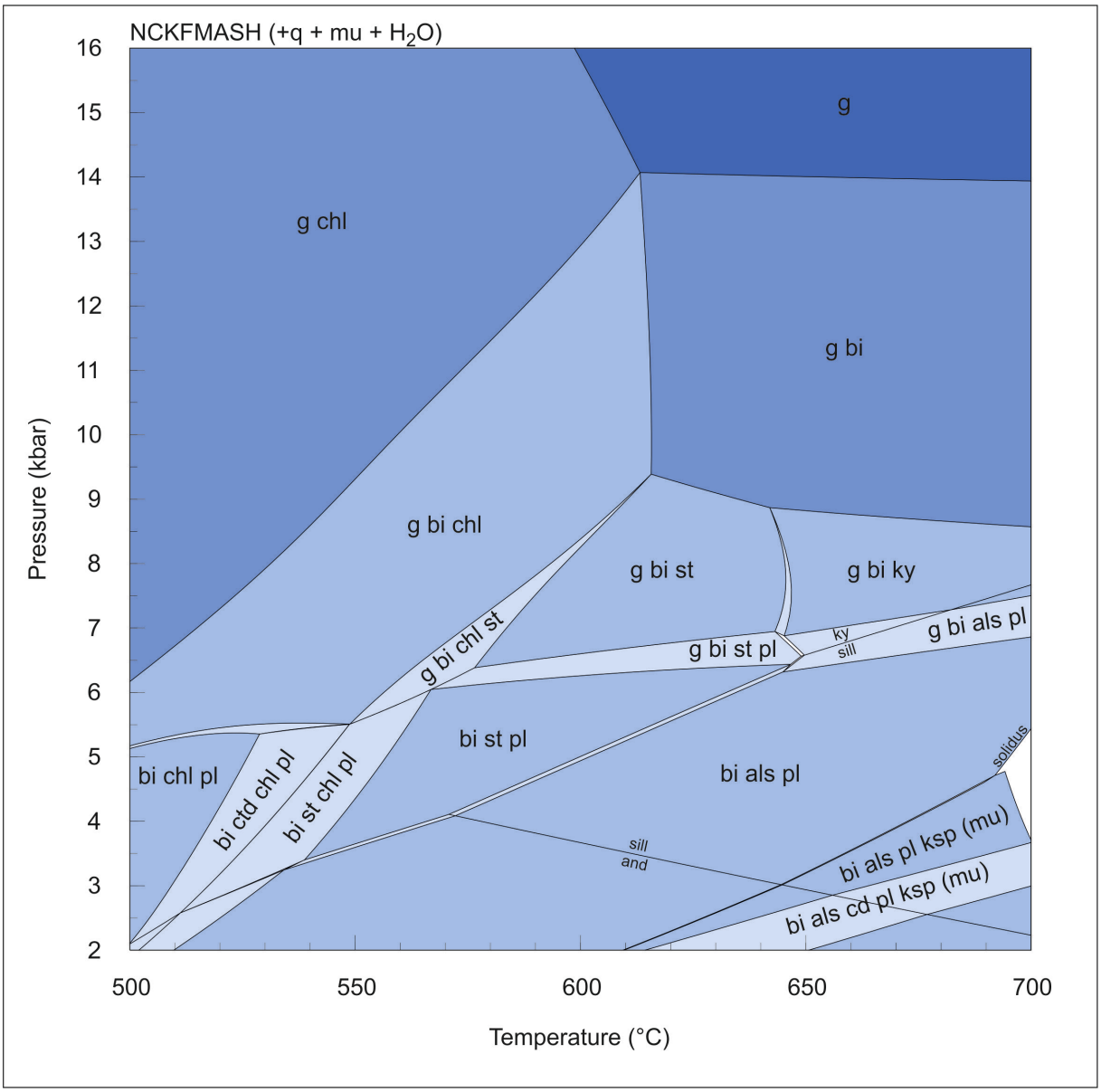

Figure 7: Pseudosection calculated with THERMOCALC for Sample AH29. The shading of the stability fields represents the variance of the respective field. Quartz, muscovite and H_2O are assumed to be in excess. The bulk composition is reported in Table (6).

6 DISCUSSION

In order to interpret the results of this study, the pressure values are put in context with previous scientific works. In the following, consequential possible interpretations for these results are reported.

6.1 Geothermobarometric results

The various approaches used for determining pressure conditions of metapelites yielded an interesting metamorphic gradient for the research area. Pressures in the Plankogel Unit including the calculated error margin reach from 5.15 kbar to 14.92 kbar, whereas only two samples yield values above 13 kbar. In the Pohorje Mountains, further south pressures seem to rise and values from 13.05 kbar to 26.39 kbar were worked out. These results are consistent with other studies and are able to complete the metamorphic field gradient of the Eastern Alps.

The rising of the pressures is not entirely regular which can be explained by the rather complex and not perfectly accurate methods of geothermobarometric calculations as well as localized deformation. Re-equilibration, decompression conditions and large error margins further complicate the interpretation.

As demonstrated before, the metapelites of the Pohorje Mountains record re-equilibration conditions as well as peak metamorphic conditions of the Eoalpine event (Janák et al., 2009, 2015). The Plankogel Unit, on the other hand, shows some remains of the Permian event within its garnet cores whereas the rest of the assemblage exhibits Eoalpine metamorphic conditions (Thöni & Miller, 2009).

Tenczer & Stüwe (2003) recorded a gradient which shows a slow decrease of pressures from the Koralpe to the North and a rather abrupt decrease towards the South. The decrease to the South can be explained by the Plankogel Unit. The high pressures determined for the SBUC (e.g. Janák et al., 2009, 2015), on the other hand, were assumed to indicate anew a rising of pressures throughout the Pohorje area. The pressures determined with geothermobarometric calculations in this study are consistent with these assumptions and can confirm the rising pressure conditions in these mountains, with the exception of the Plankogel Unit.

The pressure gradient across the Eastern Alps has been interpreted to represent a south- to eastward-dipping subduction zone (Janák et al., 2004). The Pohorje Mountains metamorphic

conditions seem to agree with this concept since they exhibit very high pressures. However, the Plankogel Unit separates the eclogite facies rocks of the Koralpe from the eclogite facies rocks of the Pohorje. This interruption in the high metamorphic field gradient leads to interesting assumptions concerning the tectonic evolution of this area. In the following, two models are discussed which attempt to explain these geothermobarometric results.

6.2 Possible interpretations

The Plankogel Unit sits at an interesting location, juxtaposing the Koralpe and the Pohorje Mountains. The two high-grade metamorphic areas are generally interpreted to share a similar tectonic history. Both of them roughly exhibit eclogite facies, are situated in a similar tectonic setting and include lenses of eclogites. The eclogite's presence can only be explained by very fast exhumation rates and still raises some questions on that matter. The rapid exhumation of the Eastern Alps is generally associated with the downward removal of a mantle and lower crustal wedge during subduction (e.g. Froitzheim et al., 2003; Tenczer & Stüwe, 2003; Janák et al., 2004, 2006).

The SBUC in the Pohorje Mountains yields pressures significantly higher than the Koralpe. The presence of diamonds and coesite in metapelites in close vicinity of the SBUC as well as in eclogites of the SBUC proves that these rocks were part of the same unit during subduction and that the SBUC is part of the Pohorje Nappe (Janák et al., 2015).

The peculiarity resides in the fact that the Plankogel Unit separates the Koralpe and Pohorje Mountains who seemingly belong together. Schorn & Stüwe (2016) suggested that the Plattengneis of the Koralpe and the Plankogel Unit are in fact both part of a shear zone representing the trace of the Eoalpine subduction zone. Taking on this theory, the first assumption one could make is that the Koralpe and Pohorje, in fact, do not share the same tectonic history.

The first model assumes that the Plattengneis Plankogel shear zone continues downwards and cuts off the Pohorje Mountains from the Koralpe. This model is represented in Figure 8.

The profile shows a schematic cross-section of the research area. The Koralpe is represented in the North including some eclogite lenses. The trace of the Plattengneis is indicated overlying the Koralpe units and connecting to the Plankogel Unit. The Plankogel Unit itself is overlain by some low-grade phyllites from the Lower Austroalpine units. Similar low-grade rocks are also present within the northern part of the Pohorje Mountains.

The trace of the subduction zone and the extracted slab are illustrated continuing downwards from the Plattengneis Plankogel shear zone. In this case, the Pohorje Mountains would not have been situated in the footwall of the subducting slab. This suggests that the Pohorje followed a different tectonic history. Due to the high pressures verified in the SBUC, the Pohorje Nappe must have been situated even deeper within the crust than the Koralpe. South of the subduction zone, another tectonic contact could potentially have hosted the Pohorje Nappe (as shown in Figure 10).

This model, however, shows some major flaws. The SBUC and eclogites within the Pohorje metapelites require in any case a rapid exhumation. In this tectonic scenario, a rapid exhumation would demand for another exhumation mechanism rather than the extraction of a slab within the subduction zone. Furthermore, the hints for the shared history of Koralpe and Pohorje cannot be discarded. The pressure values are clearly rising from North to South if the interruption of high pressure values caused by the Plankogel Unit is neglected. Lenses of eclogites, as well as marbles, are documented within both areas. Peak metamorphic ages and ages for the final exhumation stage are roughly the same in Koralpe and Pohorje and strongly speak against a separated tectonic history.

The model barely holds up against these arguments and taking its major flaws into consideration, a second model is proposed. This alternate interpretation is presented in Figure 9 and takes the similarities of Koralpe and Pohorje into account.

At first sight, this cross-section looks rather similar to the first. However, the main difference is that the Plankogel Unit is assumed to be present overlying the metapelites of the Pohorje Mountains. For this model, it is likewise assumed that the Plattengneis Plankogel shear zone represents the former Eoalpine subduction zone (Schorn & Stüwe, 2016). Presuming that the Koralpe and Pohorje Mountains share a similar Cretaceous history, both units would have to be situated structurally below the Plankogel Unit. Provided that this is the case, the current position of the Plankogel Units has to be explained.

During the Cretaceous, Koralpe and Pohorje rocks were residing in the footwall of the subduction zone. This subduction zone hosted a slab extraction which led to the loss of great amounts of material and to buoyancy-driven exhumation. The trace of the extracted slab is represented by the Plankogel Unit which never reached high-pressure conditions. The units reached mid-crustal level together shortly after the slab extraction occurred.

For this model, it is assumed that the later stage of exhumation caused by east- to north-east-directed low angle extensional shearing resulted in separate uplift of the Koralpe and Pohorje Mountains. This exhumation occurred in the Early to Middle Miocene demonstrated by apatite and zircon fission track ages of 19 – 10 Ma and K – Ar mica ages of 19 – 13 Ma from country rocks of eclogites and metaultrabasites (Fodor et al., 2002).

The current position of the Plattengneis Plankogel shear zone between the eclogite facies rocks of the Koralpe and Pohorje could be explained by a relatively young fault system running from East to West. In the cross-section in Figure 9 the major fault is assumed to be situated roughly in the area of the Drave River. Several other units, such as the Ribnica Trough and the Pohorje intrusion, obscure the exact positions of further faults.

Low-grade phyllites in the North of the Pohorje Nappe are interpreted to sit above remnants of the Plankogel Unit within the metapelites. To the South of the Pohorje, the continuation of the Plankogel Unit is indicated above the current position of the Pohorje pluton which is assumed to have intruded not only into the metapelites of the Pohorje Nappe but into the Plankogel Unit as well.

Sturdy proofs for this theory are not easy to come by. It combines, however, the attained information with existing theories and brings them into a new context. The pressures continuously rise from the Koralpe to the Pohorje, inferring deeper subduction in the South. The concept of the Plattengneis Plankogel shear zone seems plausible as well since the current position of this unit is interpreted to have been caused by later exhumation.

In summary, it can be concluded that the scenario suggesting a similar Eoalpine but a different exhumation history for the Koralpe and the Pohorje Mountains is the most consistent with the obtained data. Furthermore, this model fits in with most interpretations of previously existing studies assuming a shared Cretaceous history for both units.

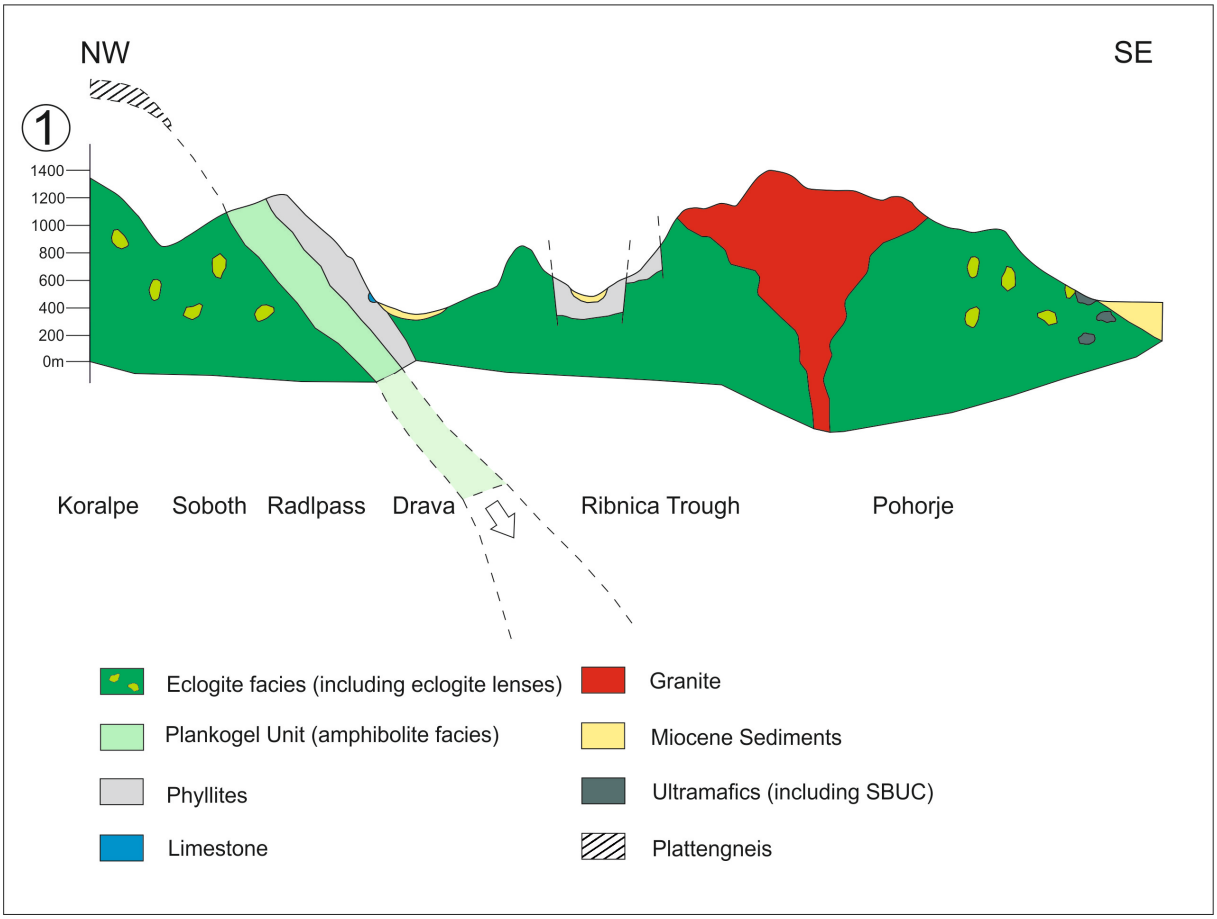

Figure 8: Visual representation of the first possible interpretation. The Plattengneis is indicated to be in connection with the Plankogel Unit. The subduction zone is indicated as a continuation of the Plankogel Unit.

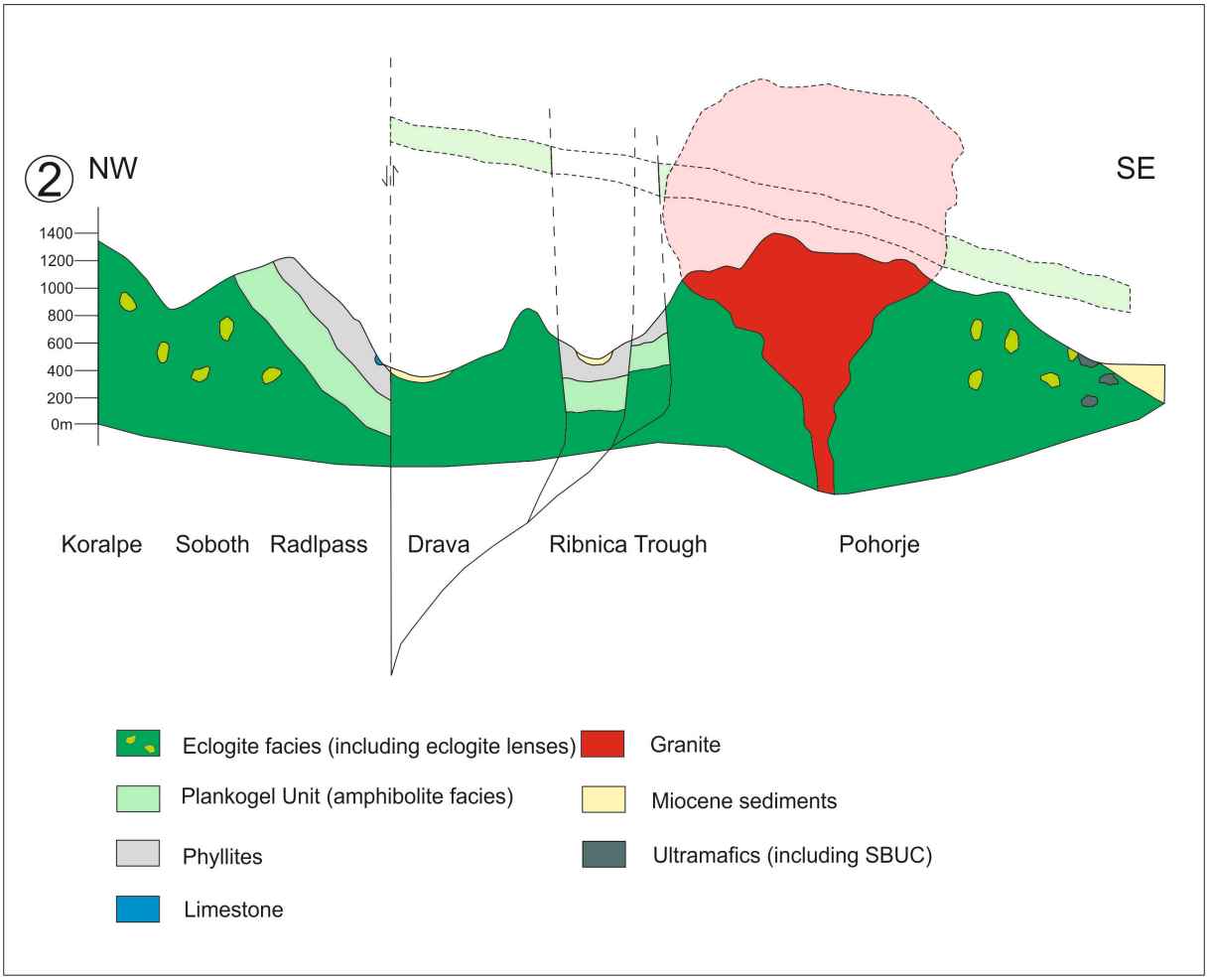

Figure 9: Visual representation of the second possible interpretation. Several faults are indicated as well as the continuation of the Plankogel Unit above the assumed position of the Pohorje pluton.

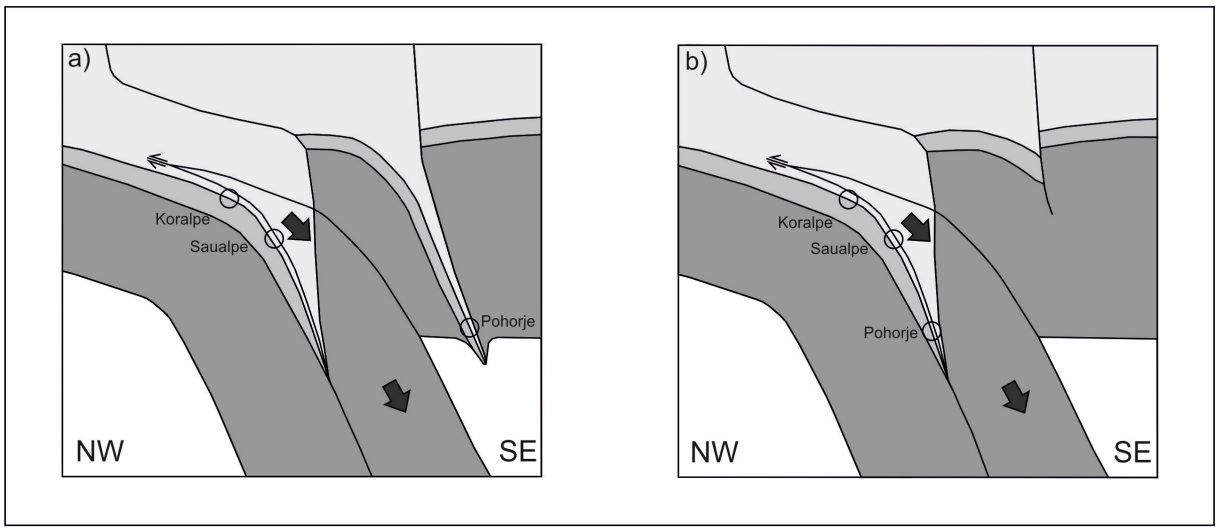

Figure 10: Simplified tectonic sketch of the Eastern Alps during Eoalpine subduction around 92 Ma (modified after Schorn & Stüwe, 2016). (a) The position of the Pohorje is separate to the Koralpe and Saualpe, independent of the Eoalpine subduction zone. (b) The Pohorje sits in the footwall of the subducted slab and is significantly deeper subducted than Koralpe and Saualpe.

7 CONCLUSION

In this study geothermobarometry has been used to constrain the tectonic and metamorphic history of the southern part of the Eastern Alps. The following results can now be concluded:

(i) Pressures to the South of the eclogite facies units of the Koralpe drop within the area of the Plankogel Unit to 7.1 ± 1.95 – 11.5 ± 3.42 kbar at an estimated temperature of 650 °C.

(ii) In the Pohorje Nappe pressures for metapelites exhibit values from 9.7 ± 2.54 kbar to 12.9 ± 1.83 kbar at 650 °C for decompression conditions and peak metamorphic pressures from 16.2 ± 3.45 kbar to 23.9 ± 2.49 kbar at 700 °C.

(iii) It is understood that the Koralpe and Pohorje Mountains were subducted together during the Eoalpine metamorphic event and subsequently exhumed due to slab extraction within the subduction zone. The Plattengneis Plankogel shear zone represents the trace of this extraction (Schorn & Stüwe, 2016).

(iv) It is suggested that the Plankogel Unit structurally overlies the eclogite facies metapelites of the Koralpe and Pohorje. Its current position is explained by a fault system emerging during the final Early to Middle Miocene exhumation caused by extensional shearing.

REFERENCES

De Hoog J.C.M., Janák M., Vrabec M. & Froitzheim N., 2009. Serpentinised peridotites from an ultrahigh-pressure terrane in the Pohorje Mts. (Eastern Alps, Slovenia): Geochemical constraints on petrogenesis and tectonic setting. *Lithos*, **109**, 209 – 222.

Eberlei T., Johnson T. E., White R. W., Roffeis C. & Stüwe K., 2014. Thermobarometric constraints on pressure variations across the Plattengneis shear zone of the Eastern Alps: implications for exhumation models during Eoalpine subduction. *Journal of Metamorphic Geology*, **32**, 227 – 244.

Fodor L.I., Jelen B., Márton E., Zupančič N., Trajanova M., Rifelj H., Pécskay Z., Balogh K., Koroknai B., Dunkl I., Horváth P., Horvat A., Vrabec M., Kraljić M. & Kevrić R., 2002. Connection of Neogene basin formation, magmatism and cooling of metamorphics in NE Slovenia. *Geologica Carpathica*, **53**, 199 – 201.

Fodor L., Balogh K., Dunkl I. et al., 2003. Structural evolution and exhumation of the Pohorje-Kozjak Mts., Slovenia. *Annales Universitatis Scientarum Budapestinensis, Sectio Geologica*, **35**, 118 – 119.

Fodor L.I., Gerdes A., Dunkl I., Koroknai B., Pécskay Z., Trajanova M., Horváth P., Vrabec M., Jelen B., Balogh K. & Frisch W., 2008. Miocene emplacement and rapid cooling of the Pohorje pluton at the Alpine-Pannonian-Dinaridic junction, Slovenia. *Swiss J. Geosci.*, **101**, 255 – 271.

Froitzheim N., Pleuger J., Roller S. & Nagel T., 2003. Exhumation of high- and ultrahigh-pressure metamorphic rocks by slab extraction. *Geology*, **31**, 925 – 928.

Froitzheim N., Pleuger J. & Nagel T., 2006. Extraction faults. *Journal of Structural Geology*, **28**, 1388 – 1395.

Froitzheim, N., Plašienka, D. & Schuster, R., 2008. Alpine tectonics of the Alps and Western Carpathians. In: The Geology of Central Europe. Volume 2: Mesozoic and Cenozoic (ed. McCann, T.), *Geological Society of London*, 1141–1232.

Gregurek D., Abart R. & Hoinkes G., 1997. Contrasting Eoalpine P-T evolutions in the southern Koralpe, Eastern Alps. *Mineralogy and Petrology*, **60**, 61 – 80.

Hinterlechner-Ravnik A., 1977. Geochemical Characteristics of the Metamorphic Rocks of the Pohorje Mountains. *Geologija*, **20**, 107 – 140.

Hinterlechner-Ravnik A., Sassi F. P. & Visona D., 1991. The Austridic eclogites, metabasites and metaultrabasites from the Pohorje area (Eastern Alps, Yugoslavia): 2. The metabasites and metaultrabasites, and concluding considerations. *Rendiconti Fisiche Accademia Lincei*, **2**, 175–190.

Hoinkes G., Koller F., Ranitsch G. et al., 1999. Alpine metamorphism of the Eastern Alps. *Schweizerische Mineralogische und Petrographische Mitteilungen*, **79**, 155–181.

Holland T.J.B. & Powell R., 1998. An internally consistent thermodynamic data set for phases of petrological interest. *Journal of Metamorphic Geology*, **16**, 309 – 343.

Hurai V., Janák M. & Thomas R., 2010. Fluid-assisted retrogression of garnet and P–T history of metapelites from HP/UHP metamorphic terrane (Pohorje Mountains, Eastern Alps). *Contrib Mineral Petrol*, **160**, 203 – 218.

Janák M., Froitzheim N., Lupták B., Vrabec M. & Krogh Ravna E.J., 2004. First evidence for ultrahigh-pressure metamorphism of eclogites in Pohorje, Slovenia: Tracing deep continental subduction in the Eastern Alps. *Tectonics*, **23**, TC5014.

Janák M., Froitzheim N., Vrabec M. & Krogh Ravna E.J., 2005. Reply to comment by C. Miller and J. Konzett on ‘‘First evidence for ultrahigh-pressure metamorphism of eclogites in Pohorje, Slovenia: Tracing deep continental subduction in the eastern Alps’’. *Tectonics*, **24**, TC6011.

Janák M., Froitzheim N., Vrabec M., Krogh Ravna E.J. & De Hoog J.C.M., 2006. Ultrahigh-pressure metamorphism and exhumation of garnet peridotite in Pohorje, Eastern Alps. *Journal of Metamorphic Geology*, **24**, 19 – 31.

Janák M., Cornell D., Froitzheim N., De Hoog J.C.M., Broska I., Vrabec M. & Hurai V., 2009. Eclogite-hosting metapelites from the Pohorje Mountains (Eastern Alps): P-T evolution, zircon geochronology and tectonic implications. *Eur. J. Mineral.*, **21**, 1191 – 1212.

Janák M., Froitzheim N., Yoshida K., Sasinková V., Nosko M., Kobayashi T., Hirajima T. & Vrabec M., 2015. Diamond in metasedimentary crustal rocks from Pohorje, Eastern Alps: a window to deep continental subduction. *Journal of Metamorphic Geology*, **33**, 495 – 512.

Jarc S. & Zupancic N., 2007. A cathodoluminescence and petrographical study of marbles from the Pohorje area in Slovenia. *Geochemistry*, **69**, 75 – 80.

Kirst F., Sandmann S., Nagel T.J., Froitzheim N. & Janák M., 2010. Tectonic evolution of the southeastern part of the Pohorje Mountains (Eastern Alps, Slovenia). *Geologica Carpathica*, **61**, 6, 451 – 461.

Kleinschmidt G., 1975. Die "Plankogelserie" in der südlichen Koralpe unter besonderer Berücksichtigung von Manganquarziten. *Verh. Geol. B.-A.*, **2 – 3**, 351 – 362.

Miller C. & Thöni M., 1997. Eo-Alpine eclogitisation of Permian MORB-type gabbros in the Koralpe (Eastern Alps, Austria) : new geochronological, geochemical and petrological data. *Chemical Geology*, **137**, 283 – 310.

Miller C., Mundil R., Thöni M. & Konzett J., 2005. Refining the timing of eclogite metamorphism: a geochemical, petrological, Sm-Nd and U-Pb case study from the Pohorje Mountains, Slovenia (Eastern Alps). *Contrib Mineral Petrol*, **150**, 70 – 84.

Miller C., Zanetti A., Thöni M. & Konzett J., 2007. Eclogitisation of gabbroic rocks: Redistribution of trace elements and Zr in rutile thermometry in an Eo-Alpine subduction zone (Eastern Alps). *Chemical Geology*, **239**, 96 – 123.

Mioč P. & Žnidarčič M., 1977. Geological map of SFRJ 1:100 000, Sheet Slovenj Gradec. *Geological Survey, Ljubljana, Federal Geological Survey, Beograd*.

Powell R. & Holland T.J.B., 1988. An internally consistent dataset with uncertainties and correlations: 3. Applications to geobarometry, worked examples and a computer program. *Journal of Metamorphic Geology*, **6**, 173 – 204.

Powell R. & Holland T.J.B., 1994. Optimal geothermometry and geobarometry. *American Mineralogist*, **79**, 120-133.

Sandmann S., Herwartz D., Kirst F., Froitzheim N., Nagel T., Fonseca R., Münker C. & Janák M., 2016. Timing of eclogite-facies metamorphism of mafic and ultramafic rocks from the Pohorje Mountains (Eastern Alps, Slovenia) based on Lu-Hf garnet geochronometry. *Lithos*, **262**, 576 – 585.

Sassi R., Mazzoli C., Miller C. & Konzett J., 2004. Geochemistry and metamorphic evolution of the Pohorje Mountain eclogites from the easternmost Austroalpine basement of the Eastern Alps (Northern Slovenia). *Lithos*, **78**, 235 – 261.

Schmid S. M., Fügenschuh B., Kissling E. & Schuster R., 2004. Tectonic map and overall architecture of the Alpine orogen. *Eclogae Geologicae Helvetiae*, **97**, 93 – 117.

Schorn S. & Stüwe K., 2016. The Plankogel detachment of the Eastern Alps: petrological evidence for an orogen-scale extraction fault. *Journal of Metamorphic Geology*, **34**, 147 – 166.

Schuster R. & Stüwe K., 2008. Permian metamorphic event in the Alps. *Geology*, **36**, 603 – 606.

Stüwe K. & Schuster R., 2010. Initiation of subduction in the Alps: Continent or ocean? *Geology*, **38**, 175 – 178.

Tenczer V. & Stüwe K., 2003. The metamorphic field gradient in the eclogite type locality, Koralpe region, Eastern Alps. *Journal of Metamorphic Geology*, **21**, 377 – 393.

Thöni M. & Jagoutz E., 1992. Some new aspects of dating eclogites in orogenic belts: Sm-Nd, Rb-Sr, and Pb-Pb isotopic results from the Austroalpine Saualpe and Koralpe type-locality (Carinthie/Styria, southeastern Austria). *Geochimica et Cosmochimica Acta*, **56**, 347 – 368.

Thöni M. & Miller C., 1996. Garnet Sm–Nd data from the Saualpe and the Koralpe (Eastern Alps, Austria): chronological and P-T constraints on the thermal and tectonic history. *Journal of Metamorphic Geology*, **14**, 453–466.

Thöni M., 2002. Sm–Nd isotope systematics in garnet from different lithologies (Eastern Alps): age results and an evaluation of potential problems for garnet Sm–Nd chronometry. *Chemical Geology*, **185**, 255–281.

Thöni M., 2006. Dating eclogites-facies metamorphism in the Eastern Alps – approaches, results, interpretations: a review. *Mineralogy and Petrology*, **88**, 123 – 148.

Thöni M. & Miller C., 2009. The "Permian event" in the Eastern European Alps: Sm-Nd and P-T data recordd by multi-stage garnet from the Plankogel unit. *Chemical Geology*, **260**, 20 – 36.

Trajanova M., Pécskay Z. & Itaya T., 2008. K-Ar geochronology and petrography of the Miocene Pohorje Mountains batholith (Slovenia). *Geologica Carpathica*, **59**, 3, 247 – 260.

Vrabec M., Janák M., Froitzheim N. & De Hoog J.C.M., 2012. Phase relations during peak metamorphism and decompression of the UHP kyanite eclogites, Pohorje Mountains (Eastern Alps, Slovenia). *Lithos*, **144 – 145**, 40 – 55.

APPENDIX

Appendix 1: Sample localities of thin-sections of metapelites, samples shown in bold were suitable for *P* calculations

Sample	Altitude (m)	Latitude	Longitude
AH1	557	46º 38.0014' N	15º 12.8333' E
AH2	365	46º 37.0887' N	15º 08.2664' E
AH3	371	46º 37.2627' N	15º 08.0986' E
AH4	445	46º 38.9063' N	15º 07.4972' E
AH5	413	46º 38.1760' N	15º 07.8985' E
AH6	314	46º 35.5111' N	15º 20.6935' E
AH7	321	46º 33.3377' N	15º 25.4155' E
AH8	579	46º 31.4149' N	15º 26.0370' E
AH9	572	46º 31.5228' N	15º 22.4512' E
AH10	740	46º 31.0752' N	15º 21.0443' E
AH11	1168	46º 26.6478' N	15º 21.5633' E
AH12	1079	46º 26.2772' N	15º 22.0582' E
AH13	774	46º 24.4183' N	15º 23.6940' E
AH14	536	46º 23.2308' N	15º 22.9378' E
AH15	495	46º 24.4006' N	15º 31.3313' E
AH16	543	46º 24.5211' N	15º 30.9669' E
AH23	935	46° 28.7431' N	15° 12.4096' E
AH28	708	46° 27.5233' N	15° 13.7209' E
AH29	585	46° 24.0053' N	15° 18.0168' E
AH30	626	46° 24.3814' N	15° 17.6278' E
AH34	766	46° 24.7172' N	15° 17.9030' E
AH38	476	46° 23.6992' N	15° 27.9156' E
AH52	1010	46° 29.2730' N	15° 31.6354' E
AH53	1108	46° 29.5546' N	15° 31.6144' E
AH56	739	46° 29.1436' N	15° 34.3654' E
AH57	222	46° 33.9836' N	15° 27.5061' E
AH61	325	46° 34.9524' N	15° 21.7620' E
AH63	828	46° 40.2869' N	15° 03.9898' E
AH64	799	46° 40.1535' N	15° 04.1898' E
AH65	887	46° 40.0319' N	15° 04.6035' E
AH66	877	46° 39.7099' N	15° 05.2319' E
AH68	1217	46° 39.4856' N	15° 03.9837' E
AH70	1266	46° 39.5488' N	15° 03.7079' E
AH74	1152	46° 40.0279' N	15° 01.9075' E
AH81	974	46° 37.1580' N	15° 02.0947' E
AH83	1131	46° 38.0296' N	15° 03.0360' E
AH87	1137	46° 38.7276' N	15° 03.7963' E
AH93	975	46° 37.7580' N	15° 04.6942' E
AH95	914	46° 37.6157' N	15° 04.7537' E
AH104	549	46° 37.7341' N	15° 03.8959' E
AH106	468	46° 36.3883' N	15° 04.8523' E
AH107	352	46° 35.1427' N	15° 14.0860' E
AH117	292	46° 35.0631' N	15° 19.6495' E

Appendix 2: End-member reactions used for barometric calculations. The phases in brackets have been assumed to be in excess. Mineral abbreviations are according to THERMOCALC.

Sample	Assemblage	Reactions	
AH68	g + mu + bi + chl + st (+ q + ky + H_2O)	12ames + 5alm + 9q = 8clin + 3daph + 2mst	3mst + 4alm = 3fst + 4py
		105ames + 55alm + 180ky = 52clin + 33daph + 40mst	48ames + 55fst + 20py + 36q = 44daph + 63mst
		297clin + 40fst = 32daph + 195ames + 235py + 360H_2O	17ames + 10east + 39q = 16clin + 2mst + 10mu
AH70	g + mu + bi + st (+ q + ky + H_2O)	3mst + 4alm = 3fst + 4py	2ann + mu + 6q = 3fcel + alm
		3east + 6q = phl + 2mu + py	2fst + 31fcel = 13ann + 18mu + 46q + 4H_2O
		31phl + 6mst = 24east + 7mu + 23py + 12H_2O	phl + east + 6q = 2cel + py
		2phl + mu + 2ky = 3east + 5q	
AH66	g + mu + st (+ q + ky H_2O)	4py + 3fst = 4alm + 3mst	39cel + 4fst = 13py + 23mu + 16fcel + 14q + 8H_2O
		3cel + 4ky = py + 3mu + 4q	8mu + 2mst + 19q = 8cel + 4H_2O + 26ky
AH87	g + mu + chl + st + ctd (+ q + ky + H_2O)	17clin + 8mst = 3ames + 72mctd + 11py	39fctd + 4alm = 7daph + 4fst + 3H_2O
		5ames + py + 4q = 3clin + 8mctd	17daph + 8fst + 6ky = 84fctd + 11alm
		ames + 2ky = 4mctd	14daph + 3fcel + 8fst = 3mu + 72fctd + 11alm
		39mctd + 4py = 7clin + 4mst + 3H_2O	ames + cel = clin + mu
		19daph + 10fst + 3q = 96fctd + 13alm	
AH83	g + mu + bi + chl + st + ctd (+ q + ky + H_2O)	39mctd + 4py = 4mst + 7clin + 3H_2O	85fctd + 11py + 3ames = 13mctd + 8mst + 17daph
		6mst + 19ames + 17q = 88mctd + 4py	14mu + 9ann + 4fctd + 34q = 23fcel + 2fst
		ames + 2ky = 4mctd	mu + 2ann + 6q = 3fcel + alm
		2mst + 13ames + 11q = 40mctd + 4clin	32mu + 10mst + 34clin = 21cel + 11phl + 156mctd
		4daph + 26ky = 12fctd + 2fst + 11q	32mu + 149cel + 10mst + 34daph = 170fcel + 11phl + 156mctd
		3daph + 10ky = 12fctd + alm + 4q	32mu + 12mctd + 17py = 25cel + 7east + 6mst
AH4	g + bi + ep + fsp (+ q + ky + H_2O)	gr + q + 2ky = 3an	3phl + 4ky = py + 3east + 4q
		2cz + q + ky = 4an + H_2O	2py + 3ann + 4ky = 3alm + 3east + 4q
AH117	g + mu + bi + chl + st (+ q + ky + H_2O)	4py + 3ames + 44ky = 6mst + 17q	6mst + 23phl + 48q = 31py + 23mu + 12H_2O
		15cel + 4mst + 6phl = 13py + 21mu + 2clin	mu + 2ann + 6q = alm + 3fcel
		21cel + 4mst + 6east = 13py + 27mu + 2clin	23fcel + 4fst = 13alm + 23mu + 14q + 8H_2O
		5py + 12mu + clin + 9q = 12cel + 2mst	3fcel + 4ky = alm + 3mu + 4q
		11py + 21mu + 4clin + 36ky = 21cel + 8mst	
AH6	g + mu + bi + fsp (+ q + ky + H_2O)	gr + q + 2ky = 3an	3phl + 4ky = py + 3east + 4q
		3east + 6q = py + phl + 2mu	2ann + mu + 6q = alm + 3fcel
		phl + east + 6q = py + 2cel	ann + q + 2ky = alm + mu
AH7	g + mu + bi + chl + fsp (+ q + ky + H_2O)	3east + 6q = py + phl + 2mu	3ann + 7q + 2ky = 2alm + 3fcel
		3phl + 4ky = py + 3east + 4q	ann + 3an = gr + alm + mu
		2east + ames + 6q = py + 2mu + clin	7gr + 5alm + 12pa + 15q = 3daph + 21an + 12ab
		cel + 2clin + 2ky = phl + 2ames + 5q	2py + 6east + 3daph + 18q = 5alm + 6cel + 3ames
		2ann + mu + 6q = alm + 3fcel	2ann + 9fcel + 14pa = 11mu + 3daph + 14ab + 2H_2O
AH9	g + mu + bi (+ q + ky + H_2O)	3east + 6q = phl + 2mu + py	2ann + mu + 6q = 3fcel + alm
		2phl + mu + 2ky = 3east + 5q	3fcel + 2ky = ann + 2mu + 5q
		phl + east + 6q = 2cel + py	
AH11	g + mu + bi + chl + fsp (+ q + ky + H_2O)	gr + q + 2ky = 3an	phl + cel + 2ky = 2east + 5q
		py + 2gr + 3ames + 6q = 3clin + 6an	2ann + mu + 6q = alm + 3fcel
		3ames + 24an = 4py + 8gr + 12H_2O + 18ky	3ann + 7q + 2ky = 2alm + 3fcel
		3east + 6q = py + phl + 2mu	9gr + 2daph + 5fcel + 16ky = 5ann + 27an + 8H_2O
		2phl + 3ames + 6q = py + 3clin + 2mu	
AH29	g + mu + bi (+ q + ky + H_2O)	3east + 6q = py + phl + 2mu	2ann + mu + 6q = alm + 3fcel
		phl + east + 6q = py + 2cel	ann + q + 2ky = alm + mu
		3phl + 4ky = py + 3east + 4q	
AH56	g + mu + bi + st (+ q + ky + H_2O)	3mst + 4alm = 3fst + 4py	phl + east + 6q = 2cel + py
		3east + 6q = phl + 2mu + py	2ann + mu + 6q = 3fcel + alm
		2phl + mu + 2ky = 3east + 5q	3fcel + 2ky = ann + 2mu + 5q
AH13	g + mu + bi (+ q + ky + H_2O)	mu + 2phl + 6q = py + 3cel	mu + 2ann + 6q = alm + 3fcel
		2east + 6q = py + mu + cel	3fcel + 4ky = alm + 3mu + 4q
		3cel + 4ky = py + 3mu + 4q	
AH38	g + mu + bi + st (+ q + ky + H_2O)	3east + 6q = py + 2mu + phl	ann + q + 2ky = alm + mu
		6mst + 31phl = 23py + 7mu + 24east + 12H_2O	6fst + 69east + 186q = 46py + 8alm + 69mu + 12H_2O
		phl + q + 2ky = py + mu	
AH63	g + mu + bi (+ q + ky + H_2O)	3east + 6q = py + phl + 2mu	2ann + mu + 6q = alm + 3fcel
		phl + east + 6q = py + 2cel	ann + q + 2ky = alm + mu
		3phl + 4ky = py + 3east + 4q	
AH57	g + mu + bi + fsp (+ q + ky + H_2O)	gr + q + 2ky = 3an	4phl + 3cel + 12ky = 5py + 7mu
		gr + 2pa + 3q = 3an + 2ab + 2H_2O	2ann + mu + 6q = alm + 3fcel
		phl + east + 6q = py + 2cel	ann + q + 2ky = alm + mu
		2phl + mu + 6q = py + 3cel	

Appendix 3: Mineral analyses used for *P* - *T* calculations

Sample	AH63		
Excess phases	qu + ky + H_2O		
Phase	Garnet	Muscovite	Biotite
Position	rim	matrix	matrix
Label	ah63_2_5	ah63_2_15	ah63_2_9
SiO_2	37.71	46.66	36.10
TiO_2	0.00	0.65	1.68
Al_2O_3	21.06	35.10	18.02
Cr_2O_3	0.10	0.06	0.11
Fe_2O_3	1.17	0.00	0.00
FeO	28.95	0.89	15.77
MnO	0.67	0.00	0.09
MgO	4.98	0.80	11.73
CaO	5.10	0.00	0.17
Na_2O	0.01	1.18	0.19
K_2O	0.00	9.71	8.16
Total	99.76	95.05	92.02
Oxygen	12.0	11.0	11.0
Si	2.981	3.097	2.776
Ti	0.000	0.033	0.097
Al	1.963	2.746	1.634
Cr	0.006	0.003	0.007
Fe^{3+}	0.070	0.000	0.000
Fe^{2+}	1.914	0.049	1.014
Mn	0.045	0.000	0.006
Mg	0.586	0.079	1.344
Ca	0.432	0.000	0.014
Na	0.002	0.151	0.029
K	0.000	0.823	0.801
Total	8.000	6.983	7.722

T [°C]	650
P [kbar]	11.5
sd [kbar]	1.36
sigfit	1.0

Appendix 3: (continuation)

Sample	AH68				
Excess phases	qu + ky + H_2O				
Phase	Garnet	Muscovite	Biotite	Chlorite	Staurolite
Position	rim	matrix	matrix	matrix	matrix
Label	ah68_2_8	ah68_2_4	ah68_2_5	ah68_5_10	ah68_3_6
SiO_2	35.74	44.57	23.79	21.90	26.07
TiO_2	0.07	0.42	0.06	0.07	0.57
Al_2O_3	20.63	36.11	21.45	20.06	51.65
Cr_2O_3	0.02	0.07	0.04	0.08	0.09
Fe_2O_3	0.00	0.00	3.49	0.00	0.00
FeO	30.38	0.69	17.81	19.61	12.26
MnO	0.03	0.00	0.00	0.01	0.03
MgO	3.16	0.57	14.37	12.90	1.42
CaO	5.22	0.01	0.00	0.02	0.02
Na_2O	0.00	2.00	0.03	0.01	0.07
K_2O	0.00	7.85	0.05	0.00	0.02
Total	95.26	92.28	81.09	74.67	92.19
Oxygen	12.0	11.0	11.0	14.0	46.0
Si	2.982	3.024	2.077	2.663	7.641
Ti	0.004	0.022	0.004	0.007	0.126
Al	2.029	2.889	2.208	2.875	17.850
Cr	0.001	0.004	0.003	0.008	0.020
Fe^{3+}	0.000	0.000	0.230	0.000	0.000
Fe^{2+}	2.120	0.039	1.301	1.994	3.005
Mn	0.002	0.000	0.000	0.001	0.009
Mg	0.393	0.058	1.870	2.337	0.618
Ca	0.467	0.000	0.000	0.003	0.007
Na	0.000	0.264	0.005	0.002	0.038
K	0.000	0.680	0.006	0.000	0.006
Total	7.999	6.980	7.704	9.890	29.320

T [°C]	650
P [kbar]	7.5
sd [kbar]	1.11
sigfit	1.0

Appendix 3: (continuation)

Sample	AH70			
Excess phases	qu + ky + H_2O			
Phase	Garnet	Muscovite	Biotite	Staurolite
Position	rim	matrix	matrix	matrix
Label	ah70_3_14	ah70_3_16	ah70_3_1	ah70_3_8
SiO_2	36.05	45.37	36.24	27.24
TiO_2	0.01	0.50	1.49	0.54
Al_2O_3	20.92	34.88	18.61	53.02
Cr_2O_3	0.07	0.01	0.10	0.00
Fe_2O_3	0.00	0.00	0.00	0.00
FeO	28.93	0.99	16.05	10.69
MnO	0.18	0.00	0.00	0.10
MgO	2.92	0.46	10.67	1.33
CaO	6.37	0.00	0.00	0.06
Na_2O	0.01	1.42	0.24	0.05
K_2O	0.00	8.71	8.39	0.00
Total	95.46	92.32	91.79	93.02
Oxygen	12.0	11.0	11.0	46.0
Si	2.989	3.088	2.794	7.822
Ti	0.001	0.025	0.086	0.116
Al	2.045	2.799	1.692	17.953
Cr	0.005	0.000	0.006	0.000
Fe^{3+}	0.000	0.000	0.000	0.000
Fe^{2+}	2.006	0.056	1.035	2.567
Mn	0.013	0.000	0.000	0.024
Mg	0.360	0.046	1.226	0.571
Ca	0.566	0.000	0.000	0.019
Na	0.002	0.187	0.036	0.026
K	0.000	0.756	0.825	0.000
Total	7.986	6.959	7.702	29.098

T [°C]	650
P [kbar]	8.8
sd [kbar]	1.21
sigfit	0.9

Appendix 3: (continuation)

Sample	AH66		
Excess phases	qu + ky + H_2O		
Phase	Garnet	Muscovite	Staurolite
Position	rim	matrix	matrix
Label	ah66_1_8	ah66_12_16	ah66_3_6
SiO_2	37.45	46.60	26.75
TiO_2	0.03	0.44	0.63
Al_2O_3	20.84	32.57	51.17
Cr_2O_3	0.00	0.00	0.00
Fe_2O_3	0.59	0.82	0.00
FeO	32.25	0.31	11.94
MnO	0.05	0.00	0.02
MgO	3.66	1.82	1.45
CaO	4.67	0.00	0.00
Na_2O	0.00	0.00	0.00
K_2O	0.00	9.23	0.00
Total	99.54	91.79	91.96
Oxygen	12.0	11.0	46.0
Si	2.997	3.179	7.833
Ti	0.002	0.023	0.139
Al	1.966	2.619	17.664
Cr	0.000	0.000	0.000
Fe^{3+}	0.035	0.042	0.000
Fe^{2+}	2.159	0.018	2.924
Mn	0.003	0.000	0.005
Mg	0.437	0.185	0.633
Ca	0.400	0.000	0.000
Na	0.000	0.000	0.000
K	0.000	0.803	0.000
Total	8.000	6.870	29.197

T [°C]	650
P [kbar]	7.1
sd [kbar]	1.95
sigfit	0.8

Appendix 3: (continuation)

Sample	AH87					
Excess phases	qu + ky + H_2O					
Phase	Garnet	Muscovite	Biotite	Chlorite	Staurolite	Chloritoid
Position	rim	matrix	matrix	matrix	matrix	matrix
Label	ah_87_21_2	ah87_21_7	ah87_21_3	ah87_21_5	ah87_21_35	ah87_21_15
SiO_2	36.63	47.07	26.56	26.07	28.62	24.38
TiO_2	0.00	0.36	0.13	0.10	0.58	0.03
Al_2O_3	20.41	35.75	23.96	24.33	53.02	40.01
Cr_2O_3	0.00	0.01	0.12	0.02	0.00	0.00
Fe_2O_3	0.91	0.00	3.87	0.00	0.00	0.00
FeO	33.25	0.93	19.71	22.61	14.18	21.35
MnO	0.03	0.00	0.00	0.00	0.05	0.00
MgO	2.68	0.37	17.84	18.25	2.27	4.12
CaO	4.42	0.00	0.00	0.00	0.03	0.00
Na_2O	0.00	1.78	0.00	0.02	0.00	0.00
K_2O	0.02	8.75	0.03	0.02	0.00	0.00
Total	98.35	95.01	92.22	91.41	98.75	89.89
Oxygen	12.0	11.0	11.0	14.0	46.0	6.0
Si	2.991	3.109	2.039	2.580	7.875	1.019
Ti	0.000	0.018	0.008	0.007	0.120	0.001
Al	1.964	2.784	2.168	2.838	17.198	1.971
Cr	0.000	0.001	0.007	0.002	0.000	0.000
Fe^{3+}	0.056	0.000	0.223	0.000	0.000	0.000
Fe^{2+}	2.270	0.051	1.265	1.871	3.262	0.746
Mn	0.002	0.000	0.000	0.000	0.012	0.000
Mg	0.326	0.037	2.041	2.691	0.930	0.257
Ca	0.387	0.000	0.000	0.000	0.007	0.000
Na	0.001	0.228	0.000	0.003	0.002	0.000
K	0.002	0.737	0.003	0.003	0.000	0.000
Total	8.000	6.964	7.755	9.996	29.407	3.994

T [°C]	650
P [kbar]	11.5
sd [kbar]	3.42
sigfit	2.8

Appendix 3: (continuation)

Sample	AH83					
Excess phases	qu + ky + H_2O					
Phase	Garnet	Muscovite	Biotit	Chlorit	Staurolit	Chloritoid
Position	rim	matrix	matrix	matrix	matrix	matrix
Label	ah83_11_6	ah83_12_3	ah83_12_6	ah83_11_7	ah83_12_18	ah83_12_9
SiO_2	38.21	48.78	37.23	26.66	28.57	25.31
TiO_2	0.05	0.39	1.41	0.15	0.38	0.01
Al_2O_3	21.86	38.21	20.03	24.01	56.72	42.67
Cr_2O_3	0.00	0.03	0.00	0.00	0.04	0.00
Fe_2O_3	0.00	0.00	0.00	0.00	0.00	0.00
FeO	37.25	0.96	19.59	24.64	14.54	23.38
MnO	0.63	0.01	0.02	0.00	0.03	0.09
MgO	2.94	0.27	10.52	14.23	2.01	3.20
CaO	1.92	0.01	0.01	0.03	0.02	0.00
Na_2O	0.02	1.87	0.29	0.03	0.00	0.00
K_2O	0.00	8.62	9.07	0.25	0.03	0.03
Total	102.88	99.15	98.18	90.02	102.34	94.70
Oxygen	12.0	11.0	11.0	14.0	46.0	6.0
Si	2.991	3.079	2.727	2.704	7.584	1.009
Ti	0.003	0.019	0.078	0.012	0.075	0.000
Al	2.018	2.843	1.730	2.871	17.750	2.005
Cr	0.000	0.001	0.000	0.000	0.009	0.000
Fe^{3+}	0.000	0.000	0.000	0.000	0.000	0.000
Fe^{2+}	2.439	0.051	1.200	2.090	3.228	0.779
Mn	0.042	0.001	0.001	0.000	0.008	0.003
Mg	0.343	0.025	1.148	2.151	0.794	0.190
Ca	0.161	0.001	0.001	0.003	0.006	0.000
Na	0.003	0.228	0.041	0.006	0.000	0.000
K	0.000	0.694	0.848	0.033	0.010	0.002
Total	7.999	6.942	7.775	9.869	29.466	3.989

T [°C]	650
P [kbar]	12.5
sd [kbar]	1.29
sigfit	1.9

Appendix 3: (continuation)

Sample	AH4			
Excess phases	qu + ky + H_2O			
Phase	Garnet	Biotite	Epidote	Feldspar
Position	rim	matrix	matrix	matrix
Label	ah4_4_8	ah4_4_9	ah4_4_17	ah4_8_3
SiO_2	37.72	37.94	39.81	59.79
TiO_2	0.00	1.78	0.03	0.00
Al_2O_3	20.60	18.34	32.35	24.04
Cr_2O_3	0.00	0.00	0.00	0.00
Fe_2O_3	0.00	0.00	1.62	0.09
FeO	26.24	17.02	0.01	0.00
MnO	1.40	0.13	0.00	0.02
MgO	2.85	10.66	0.35	0.00
CaO	8.85	0.00	23.68	6.71
Na_2O	0.00	0.00	0.00	0.00
K_2O	0.05	9.22	0.00	0.05
Total	97.71	95.09	97.85	90.70
Oxygen	12.0	11.0	12.5	8.0
Si	3.043	2.837	3.023	2.823
Ti	0.000	0.100	0.002	0.000
Al	1.959	1.617	2.896	1.338
Cr	0.000	0.000	0.000	0.000
Fe^{3+}	0.000	0.000	0.092	0.003
Fe^{2+}	1.770	1.064	0.001	0.000
Mn	0.096	0.008	0.000	0.001
Mg	0.343	1.188	0.040	0.000
Ca	0.765	0.000	1.927	0.339
Na	0.000	0.000	0.000	0.000
K	0.005	0.880	0.000	0.003
Total	7.980	7.695	7.982	4.508

T [°C]	650
P [kbar]	9.4
sd [kbar]	0.23
sigfit	0.4

Appendix 3: (continuation)

Sample	AH6			
Excess phases	qu + ky + H_2O			
Phase	Garnet	Muscovite	Biotite	Feldspar
Position	rim	matrix	matrix	matrix
Label	ah6_3x_10	ah6_1_17	ah6_3x_9	ah6_3x_4
SiO_2	37.81	47.51	36.84	63.96
TiO_2	0.09	0.96	1.72	0.07
Al_2O_3	20.88	32.66	16.72	22.52
Cr_2O_3	0.00	0.00	0.00	0.00
Fe_2O_3	0.00	0.00	0.00	0.07
FeO	27.26	1.20	15.56	0.00
MnO	0.83	0.01	0.12	0.00
MgO	4.13	1.18	11.88	0.02
CaO	7.59	0.00	0.00	4.38
Na_2O	0.00	0.00	0.00	0.00
K_2O	0.00	9.52	9.82	0.04
Total	98.59	93.04	92.66	91.06
Oxygen	12.0	11.0	11.0	8.0
Si	3.015	3.205	2.835	2.963
Ti	0.005	0.049	0.100	0.002
Al	1.963	2.597	1.517	1.230
Cr	0.000	0.000	0.000	0.000
Fe^{3+}	0.000	0.000	0.000	0.002
Fe^{2+}	1.818	0.068	1.002	0.000
Mn	0.056	0.001	0.008	0.000
Mg	0.491	0.119	1.363	0.001
Ca	0.649	0.000	0.000	0.217
Na	0.000	0.000	0.000	0.000
K	0.000	0.819	0.964	0.002
Total	7.998	6.858	7.789	4.419

T [°C]	650
P [kbar]	9.1
sd [kbar]	0.56
sigfit	0.7

Appendix 3: (continuation)

Sample	AH117				
Excess phases	qu + ky + H_2O				
Phase	Garnet	Muscovite	Biotite	Chlorite	Staurolite
Position	rim	matrix	matrix	matrix	matrix
Label	ah117_2_8	ah117_2_15	ah117_3_13	ah117_3_10	ah117_2_6
SiO_2	37.24	45.33	35.16	24.26	28.15
TiO_2	0.12	0.59	1.67	0.03	0.70
Al_2O_3	20.52	33.13	17.29	20.44	51.73
Cr_2O_3	0.05	0.00	0.11	0.01	0.00
Fe_2O_3	2.47	0.00	2.75	0.00	0.00
FeO	31.90	1.30	20.02	30.19	9.20
MnO	0.43	0.02	0.13	0.24	0.17
MgO	4.80	1.15	8.79	11.40	1.01
CaO	2.87	0.06	0.05	0.00	0.01
Na_2O	0.00	1.62	0.12	0.00	0.13
K_2O	0.02	8.54	7.79	0.00	0.06
Total	100.42	91.74	93.88	86.57	91.17
Oxygen	12.0	11.0	11.0	14.0	46.0
Si	2.958	3.116	2.729	2.671	8.177
Ti	0.007	0.031	0.097	0.003	0.153
Al	1.922	2.685	1.582	2.653	17.715
Cr	0.003	0.000	0.007	0.001	0.000
Fe^{3+}	0.147	0.000	0.161	0.000	0.000
Fe^{2+}	2.119	0.075	1.299	2.780	2.235
Mn	0.029	0.001	0.009	0.022	0.043
Mg	0.568	0.117	1.017	1.870	0.438
Ca	0.245	0.004	0.004	0.000	0.004
Na	0.000	0.216	0.019	0.000	0.076
K	0.002	0.749	0.772	0.000	0.021
Total	8.000	6.994	7.695	10.000	28.861

T [°C]	650
P [kbar]	12.9
sd [kbar]	1.83
sigfit	2.0

Appendix 3: (continuation)

Sample	AH7				
Excess phases	qu + ky + H_2O				
Phase	Garnet	Muscovite	Biotite	Chlorite	Feldspar
Position	rim	matrix	matrix	matrix	matrix
Label	ah7_1_11	ah7_1_17	ah7_1_18	ah7_2_5	ah7_4_2
SiO_2	38.33	48.08	36.43	24.91	64.88
TiO_2	0.01	1.09	1.71	0.17	0.07
Al_2O_3	21.31	32.32	16.64	20.61	23.39
Cr_2O_3	0.10	0.06	0.09	0.03	0.01
Fe_2O_3	1.60	0.00	0.00	0.00	0.00
FeO	25.70	1.68	18.73	28.28	0.00
MnO	0.63	0.00	0.12	0.40	0.00
MgO	3.99	1.83	10.87	12.92	0.00
CaO	9.54	0.00	0.04	0.02	4.27
Na_2O	0.04	0.81	0.09	0.00	9.31
K_2O	0.00	10.32	9.55	0.04	0.11
Total	101.24	96.20	94.27	87.36	102.03
Oxygen	12.0	11.0	11.0	14.0	8.0
Si	2.977	3.176	2.800	2.686	2.807
Ti	0.000	0.054	0.099	0.013	0.002
Al	1.951	2.517	1.508	2.620	1.193
Cr	0.006	0.003	0.005	0.002	0.000
Fe^{3+}	0.094	0.000	0.000	0.000	0.000
Fe^{2+}	1.669	0.093	1.204	2.551	0.000
Mn	0.041	0.000	0.008	0.036	0.000
Mg	0.462	0.180	1.245	2.076	0.000
Ca	0.794	0.000	0.003	0.002	0.198
Na	0.006	0.104	0.013	0.000	0.781
K	0.000	0.870	0.936	0.005	0.006
Total	8.000	6.997	7.821	9.992	4.987

T [°C]	650
P [kbar]	9.7
sd [kbar]	2.00
sigfit	3.7

Appendix 3: (continuation)

Sample	AH57			
Excess phases	qu + ky + H_2O			
Phase	Garnet	Muscovite	Biotite	Feldspar
Position	matrix	matrix	matrix	matrix
Label	ah57_3_4	ah57_3_13	ah57_3_9	ah57_3_3
SiO_2	37.28	48.61	24.94	64.66
TiO_2	0.02	0.88	0.62	0.02
Al_2O_3	20.74	33.30	19.28	23.12
Cr_2O_3	0.07	0.00	0.00	0.01
Fe_2O_3	0.16	0.00	4.27	0.11
FeO	31.46	1.21	21.75	0.00
MnO	0.59	0.00	0.26	0.00
MgO	3.78	1.36	12.31	0.00
CaO	4.26	0.03	0.00	4.00
Na_2O	0.02	1.18	0.02	8.49
K_2O	0.08	9.49	0.91	0.03
Total	98.47	96.06	84.35	100.43
Oxygen	12.0	11.0	11.0	8.0
Si	3.010	3.188	2.159	2.828
Ti	0.001	0.043	0.041	0.001
Al	1.974	2.575	1.967	1.192
Cr	0.004	0.000	0.000	0.000
Fe^{3+}	0.010	0.000	0.278	0.004
Fe^{2+}	2.125	0.066	1.575	0.000
Mn	0.040	0.000	0.019	0.000
Mg	0.455	0.133	1.588	0.000
Ca	0.369	0.002	0.000	0.187
Na	0.003	0.150	0.004	0.720
K	0.008	0.794	0.100	0.001
Total	8.000	6.954	7.730	4.934

T [°C]	650
P [kbar]	10.1
sd [kbar]	1.55
sigfit	2.9

Appendix 3: (continuation)

Sample	AH9		
Excess phases	qu + ky + H_2O		
Phase	Garnet	Muscovite	Biotite
Position	matrix	matrix	matrix
Label	ah9_1_17	ah9_1_5	ah9_1_3
SiO_2	37.33	46.04	37.38
TiO_2	0.12	1.45	1.71
Al_2O_3	20.72	33.42	16.94
Cr_2O_3	0.05	0.05	0.13
Fe_2O_3	1.01	0.00	0.00
FeO	31.35	1.50	17.17
MnO	0.68	0.00	0.12
MgO	2.81	1.34	10.72
CaO	5.99	0.04	0.12
Na_2O	0.00	0.46	0.09
K_2O	0.00	10.72	8.54
Total	100.08	95.03	92.92
Oxygen	12.0	11.0	11.0
Si	2.984	3.088	2.865
Ti	0.007	0.073	0.098
Al	1.953	2.643	1.531
Cr	0.003	0.003	0.008
Fe^{3+}	0.061	0.000	0.000
Fe^{2+}	2.096	0.084	1.101
Mn	0.046	0.000	0.007
Mg	0.335	0.134	1.225
Ca	0.513	0.003	0.010
Na	0.000	0.059	0.013
K	0.000	0.917	0.835
Total	8.000	7.005	7.692

T [°C]	650
P [kbar]	11.7
sd [kbar]	1.73
sigfit	1.3

Appendix 3: (continuation)

Sample	AH28	
Excess phases	qu + ky + H_2O	
Phase	Garnet	Muscovite
Position	rim	matrix
Label	ah28_2_5	ah28_1_22
SiO_2	38.32	46.33
TiO_2	0.06	0.43
Al_2O_3	20.91	32.43
Cr_2O_3	0.00	0.00
Fe_2O_3	2.39	0.00
FeO	21.17	1.27
MnO	1.04	0.05
MgO	7.61	1.57
CaO	7.85	0.01
Na_2O	0.00	0.00
K_2O	0.01	10.20
Total	99.36	92.29
Oxygen	12.0	11.0
Si	2.972	3.173
Ti	0.003	0.022
Al	1.912	2.618
Cr	0.000	0.000
Fe^{3+}	0.139	0.000
Fe^{2+}	1.373	0.073
Mn	0.068	0.003
Mg	0.879	0.160
Ca	0.652	0.001
Na	0.000	0.000
K	0.001	0.891
Total	8.000	6.942

T [°C]	650
P [kbar]	9.7
sd [kbar]	2.54
sigfit	0.8

Appendix 3: (continuation)

Sample	AH11				
Excess phases	qu + ky + H_2O				
Phase	Garnet	Muscovite	Biotite	Chlorite	Feldspar
Position	matrix	matrix	matrix	matrix	matrix
Label	ah11_1_9	ah11_1_25	ah11_5_18	ah11_7_10	ah11_7_6
SiO_2	37.61	47.99	34.53	25.12	38.94
TiO_2	0.11	0.91	1.58	0.04	0.06
Al_2O_3	20.80	31.38	17.33	20.92	31.64
Cr_2O_3	0.00	0.06	0.02	0.00	0.08
Fe_2O_3	2.26	0.00	1.83	0.00	1.13
FeO	24.34	1.60	17.89	24.38	0.00
MnO	0.54	0.01	0.16	0.32	0.09
MgO	6.17	2.17	10.26	15.22	0.07
CaO	7.13	0.00	0.08	0.02	23.02
Na_2O	0.01	0.65	0.14	0.03	0.08
K_2O	0.00	9.60	8.45	0.00	0.03
Total	98.97	94.37	92.29	86.06	95.13
Oxygen	12.0	11.0	11.0	14.0	8.0
Si	2.962	3.214	2.709	2.690	1.944
Ti	0.007	0.046	0.093	0.004	0.002
Al	1.931	2.478	1.603	2.642	1.862
Cr	0.000	0.003	0.001	0.000	0.003
Fe^{3+}	0.134	0.000	0.108	0.000	0.042
Fe^{2+}	1.603	0.090	1.174	2.184	0.000
Mn	0.036	0.000	0.011	0.029	0.004
Mg	0.725	0.216	1.200	2.429	0.005
Ca	0.602	0.000	0.007	0.003	1.231
Na	0.001	0.085	0.022	0.007	0.008
K	0.000	0.820	0.846	0.000	0.002
Total	8.000	6.953	7.776	9.988	5.104

T [°C]	650
P [kbar]	9.8
sd [kbar]	1.60
sigfit	2.7

Appendix 3: (continuation)

Sample	AH56			
Excess phases	qu + ky + H_2O			
Phase	Garnet	Muscovite	Biotite	Staurolite
Position	rim	matrix	matrix	matrix
Label	ah56_4_1	ah56_2_6	ah56_2_2	ah56_2_12
SiO_2	37.96	46.95	36.75	28.02
TiO_2	0.01	0.45	1.75	0.54
Al_2O_3	22.35	37.78	20.06	56.44
Cr_2O_3	0.07	0.02	0.00	0.02
Fe_2O_3	0.06	0.00	0.00	0.00
FeO	35.08	0.88	20.40	14.25
MnO	0.67	0.00	0.09	0.14
MgO	4.74	0.29	8.58	1.56
CaO	0.93	0.03	0.11	0.00
Na_2O	0.00	1.74	0.28	0.01
K_2O	0.00	9.14	9.00	0.02
Total	101.89	97.29	97.03	101.00
Oxygen	12.0	11.0	11.0	46.0
Si	2.966	3.035	2.738	7.535
Ti	0.001	0.022	0.098	0.109
Al	2.059	2.880	1.762	17.892
Cr	0.005	0.001	0.000	0.004
Fe^{3+}	0.004	0.000	0.000	0.000
Fe^{2+}	2.292	0.048	1.271	3.204
Mn	0.045	0.000	0.006	0.031
Mg	0.552	0.028	0.952	0.625
Ca	0.078	0.002	0.009	0.000
Na	0.000	0.218	0.041	0.007
K	0.000	0.754	0.855	0.008
Total	8.000	6.989	7.732	29.415

T [°C]	650
P [kbar]	9.6
sd [kbar]	1.80
sigfit	0.9

Appendix 3: (continuation)

Sample	AH29		
Excess phases	qu + ky + H_2O		
Phase	Garnet	Muscovite	Biotite
Position	rim	matrix	matrix
Label	ah29_7_2	ah29_7_7	ah29_7_5
SiO_2	37.70	47.86	36.88
TiO_2	0.04	0.72	0.65
Al_2O_3	21.83	31.59	18.71
Cr_2O_3	0.00	0.00	0.00
Fe_2O_3	0.87	1.26	1.92
FeO	30.61	0.49	15.73
MnO	0.43	0.00	0.00
MgO	5.46	2.05	11.92
CaO	3.24	0.03	0.00
Na_2O	0.00	0.00	0.00
K_2O	0.06	9.06	8.50
Total	100.25	93.06	94.31
Oxygen	12.0	11.0	11.0
Si	2.963	3.223	2.772
Ti	0.002	0.036	0.037
Al	2.023	2.508	1.658
Cr	0.000	0.000	0.000
Fe^{3+}	0.052	0.064	0.109
Fe^{2+}	2.013	0.027	0.989
Mn	0.029	0.000	0.000
Mg	0.640	0.206	1.335
Ca	0.273	0.002	0.000
Na	0.000	0.000	0.000
K	0.006	0.778	0.815
Total	8.000	6.845	7.716

T [°C]	650
P [kbar]	11.2
sd [kbar]	1.42
sigfit	1.0

Appendix 3: (continuation)

Sample	AH13		
Excess phases	qu + ky + H_2O		
Phase	Garnet	Muscovite	Biotite
Position	matrix	matrix	matrix
Label	ah13_21_4	ah13_21_6	ah13_21_10
SiO_2	36.72	50.20	32.33
TiO_2	0.00	0.54	0.07
Al_2O_3	20.51	33.43	20.26
Cr_2O_3	0.00	0.00	0.00
Fe_2O_3	1.28	0.75	3.62
FeO	32.97	0.83	18.46
MnO	1.10	0.03	0.24
MgO	3.38	1.50	11.14
CaO	2.89	0.00	0.38
Na_2O	0.00	0.00	0.00
K_2O	0.03	9.31	0.44
Total	98.89	96.60	86.94
Oxygen	12.0	11.0	11.0
Si	2.981	3.247	2.584
Ti	0.000	0.026	0.004
Al	1.963	2.549	1.909
Cr	0.000	0.000	0.000
Fe^{3+}	0.078	0.037	0.218
Fe^{2+}	2.239	0.045	1.234
Mn	0.076	0.002	0.016
Mg	0.409	0.145	1.327
Ca	0.251	0.000	0.033
Na	0.000	0.000	0.000
K	0.003	0.768	0.045
Total	8.000	6.819	7.370

T [°C]	650
P [kbar]	12.3
sd [kbar]	2.25
sigfit	1.3

Appendix 3: (continuation)

Sample	AH38			
Excess phases	qu + ky + H_2O			
Phase	Garnet	Muscovite	Biotite	Staurolite
Position	matrix	matrix	matrix	matrix
Label	ah38_2_2	ah38_1_7	ah38_1_12	ah38_12_1
SiO_2	36.23	47.78	34.81	27.22
TiO_2	0.08	0.59	1.71	0.63
Al_2O_3	20.11	36.66	19.22	53.40
Cr_2O_3	0.00	0.00	0.00	0.00
Fe_2O_3	1.53	0.62	0.00	0.00
FeO	34.26	0.24	18.18	13.21
MnO	0.97	0.03	0.08	0.32
MgO	4.23	0.58	8.00	1.63
CaO	0.48	0.00	0.03	0.00
Na_2O	0.00	0.00	0.00	0.00
K_2O	0.00	7.98	8.19	0.02
Total	97.88	94.48	90.22	96.43
Oxygen	12.0	11.0	11.0	46.0
Si	2.975	3.125	2.762	7.654
Ti	0.005	0.029	0.102	0.133
Al	1.947	2.827	1.798	17.703
Cr	0.000	0.000	0.000	0.000
Fe^{3+}	0.094	0.031	0.000	0.000
Fe^{2+}	2.352	0.013	1.206	3.107
Mn	0.067	0.002	0.005	0.076
Mg	0.518	0.057	0.946	0.683
Ca	0.042	0.000	0.003	0.000
Na	0.000	0.000	0.000	0.000
K	0.000	0.666	0.829	0.007
Total	8.000	6.750	7.652	29.364

T [°C]	650
P [kbar]	10.9
sd [kbar]	1.70
sigfit	1.0

Appendix 4: Mineral analyses used for peak *P* - *T* calculations

Sample	AH6		AH117		AH7	
Excess phases	qu + ky		qu + ky		qu + ky	
Phase	Garnet	Muscovite	Garnet	Muscovite	Garnet	Muscovite
Position	core	matrix	core	matrix	core	matrix
Label	ah6_3_2	ah6_1_14	ah117_2_9	ah117_2_12	ah7_1_3	ah7_2_9
SiO_2	37.27	47.61	37.17	46.72	38.22	48.70
TiO_2	0.00	0.80	0.10	0.65	0.00	0.66
Al_2O_3	20.76	32.71	20.67	34.48	21.13	32.14
Cr_2O_3	0.00	0.00	0.02	0.03	0.03	0.00
Fe_2O_3	0.00	0.24	3.18	0.00	1.86	0.00
FeO	28.41	0.94	31.29	0.91	27.59	1.69
MnO	6.36	0.03	0.41	0.00	0.92	0.00
MgO	3.07	1.63	5.23	0.53	2.69	1.84
CaO	2.77	0.08	2.70	0.03	9.37	0.02
Na_2O	0.00	0.00	0.00	1.97	0.05	0.66
K_2O	0.00	9.61	0.02	8.62	0.04	10.62
Total	98.64	93.65	100.78	93.95	101.91	96.33
Oxygen	12.0	11.0	12.0	11.0	12.0	11.0
Si	3.023	3.193	2.937	3.125	2.979	3.211
Ti	0.000	0.040	0.006	0.033	0.000	0.033
Al	1.985	2.587	1.925	2.719	1.942	2.498
Cr	0.000	0.000	0.001	0.002	0.002	0.000
Fe^{3+}	0.000	0.012	0.189	0.000	0.109	0.000
Fe^{2+}	1.927	0.053	2.068	0.051	1.799	0.093
Mn	0.437	0.002	0.027	0.000	0.061	0.000
Mg	0.371	0.163	0.615	0.053	0.313	0.181
Ca	0.241	0.006	0.229	0.002	0.783	0.001
Na	0.000	0.000	0.000	0.255	0.008	0.084
K	0.000	0.822	0.002	0.735	0.004	0.894
Total	7.984	6.879	8.000	6.977	8.000	6.997

T [°C]	700	700	700
P [kbar]	16.2	21.3	22.2
sd [kbar]	3.45	2.72	2.38
sigfit	1.0	1.2	0.1

Appendix 4: (continuation)

Sample	AH9		AH11	
Excess phases	qu + ky		qu + ky	
Phase	Garnet	Muscovite	Garnet	Muscovite
Position	core	matrix	core	matrix
Label	ah9_3_9	ah9_1_5	ah11_5_9	ah11_1_24
SiO_2	36.99	46.04	37.44	49.32
TiO_2	0.06	1.45	0.08	0.88
Al_2O_3	20.28	33.42	20.71	30.77
Cr_2O_3	0.00	0.05	0.01	0.14
Fe_2O_3	1.64	0.00	1.55	0.00
FeO	29.26	1.50	23.31	1.61
MnO	7.52	0.00	0.71	0.00
MgO	2.79	1.34	5.22	2.45
CaO	1.67	0.04	8.95	0.00
Na_2O	0.01	0.46	0.01	0.73
K_2O	0.09	10.72	0.00	9.54
Total	100.31	95.03	97.97	95.44
Oxygen	12.0	11.0	12.0	11.0
Si	2.986	3.088	2.978	3.261
Ti	0.003	0.073	0.005	0.044
Al	1.930	2.643	1.942	2.399
Cr	0.000	0.003	0.001	0.007
Fe^{3+}	0.100	0.000	0.093	0.000
Fe^{2+}	1.976	0.084	1.551	0.089
Mn	0.514	0.000	0.048	0.000
Mg	0.336	0.134	0.619	0.242
Ca	0.144	0.003	0.763	0.000
Na	0.001	0.059	0.001	0.093
K	0.009	0.917	0.000	0.805
Total	8.000	7.005	8.000	6.941

T [°C]	700	700
P [kbar]	18.1	23.9
sd [kbar]	2.84	2.49
sigfit	0.9	0.1

Appendix 4: (continuation)

Sample	AH29		AH13	
Excess phases	qu + ky		qu + ky	
Phase	Garnet	Muscovite	Garnet	Muscovite
Position	core	matrix	core	matrix
Label	ah29_7_16	ah29_2_12	ah13_21_24	ah13_21_7
SiO_2	38.18	48.43	37.30	49.04
TiO_2	0.00	0.75	0.01	0.66
Al_2O_3	21.50	31.14	20.56	32.81
Cr_2O_3	0.00	0.00	0.00	0.00
Fe_2O_3	0.00	1.16	0.03	0.00
FeO	32.04	0.45	33.16	1.33
MnO	0.40	0.02	1.46	0.15
MgO	4.13	2.15	2.63	1.57
CaO	4.06	0.00	4.12	0.00
Na_2O	0.00	0.00	0.00	0.00
K_2O	0.03	9.32	0.00	9.81
Total	100.34	93.42	99.27	95.37
Oxygen	12.0	11.0	12.0	11.0
Si	3.013	3.250	3.018	3.232
Ti	0.000	0.038	0.001	0.033
Al	2.001	2.464	1.961	2.549
Cr	0.000	0.000	0.000	0.000
Fe^{3+}	0.000	0.059	0.002	0.000
Fe^{2+}	2.115	0.025	2.244	0.073
Mn	0.027	0.001	0.100	0.008
Mg	0.486	0.215	0.317	0.154
Ca	0.343	0.000	0.357	0.000
Na	0.000	0.000	0.000	0.000
K	0.003	0.798	0.000	0.825
Total	7.988	6.850	8.000	6.874

T [°C]	700	700
P [kbar]	18.6	17.5
sd [kbar]	3.58	4.06
sigfit	1.1	1.3

Appendix 5: Mineral analyses of garnet porphyroblast in Sample AH87 of the Plankogel Unit

Sample	AH87								
Phase	garnet								
Position	ah_87_23_1	ah_87_23_2	ah_87_23_3	ah_87_23_4	ah_87_23_5	ah_87_23_6	ah_87_23_7	ah_87_23_8	ah_87_23_9
Label	rim	rim	rim	core	core	core	rim	rim	rim
SiO_2	37.62	37.45	37.47	37.43	36.21	36.99	36.93	37.17	36.83
TiO_2	0.03	0.06	0.00	0.00	0.00	0.00	0.01	0.07	0.01
Al_2O_3	20.52	20.56	20.50	20.39	20.37	20.30	20.64	20.57	20.44
Cr_2O_3	0.06	0.01	0.02	0.00	0.05	0.00	0.00	0.09	0.00
Fe_2O_3	0.86	0.00	1.83	1.65	1.47	1.78	1.02	2.11	1.30
FeO	32.87	32.68	31.80	37.42	37.92	36.31	35.46	34.18	34.84
MnO	0.00	0.05	0.32	0.64	1.03	1.01	0.91	1.43	1.41
MgO	3.37	2.48	2.99	2.45	1.51	2.18	1.97	2.46	1.83
CaO	4.72	5.82	5.65	1.65	1.28	2.20	3.34	3.44	3.38
Na_2O	0.00	0.01	0.02	0.04	0.00	0.00	0.00	0.02	0.04
K_2O	0.03	0.00	0.01	0.01	0.00	0.06	0.00	0.00	0.00
Totals	100.07	99.12	100.61	101.67	99.85	100.84	100.26	101.54	100.07
Oxygens	12.0	12.0	12.0	12.0	12.0	12.0	12.0	12.0	12.0
Si	3.006	3.023	2.984	2.993	2.969	2.984	2.985	2.965	2.986
Ti	0.002	0.004	0.000	0.000	0.000	0.000	0.000	0.004	0.001
Al	1.933	1.956	1.925	1.922	1.969	1.931	1.967	1.933	1.954
Cr	0.004	0.000	0.001	0.000	0.004	0.000	0.000	0.006	0.000
Fe^{3+}	0.052	0.000	0.110	0.099	0.091	0.108	0.062	0.126	0.079
Fe^{2+}	2.196	2.206	2.118	2.502	2.600	2.449	2.397	2.280	2.363
Mn	0.000	0.003	0.022	0.043	0.071	0.069	0.063	0.097	0.097
Mg	0.401	0.299	0.355	0.292	0.185	0.263	0.237	0.292	0.221
Ca	0.404	0.503	0.482	0.141	0.113	0.190	0.289	0.294	0.293
Na	0.000	0.002	0.003	0.006	0.000	0.000	0.000	0.003	0.006
K	0.003	0.000	0.001	0.001	0.000	0.006	0.000	0.000	0.000
Sum	8.000	7.996	8.000	8.000	8.000	8.000	8.000	8.000	8.000